RESEARCH ARTICLE | DECEMBER 08 2023

Further extension of the Madrid-2019 force field: Parametrization of nitrate (NO_3^-) and ammonium (NH_4^+) ions

Víctor M. Trejos ; Marcos de Lucas ; Carlos Vega ; Samuel Blazquez ; Francisco Gámez

J. Chem. Phys. 159, 224501 (2023)
https://doi.org/10.1063/5.0177363

The Journal of Chemical Physics ARTICLE pubs.aip.org/aip/jcp

Further extension of the Madrid-2019 force field: Parametrization of nitrate (NO_3^-) and ammonium (NH_4^+) ions

Cite as: J. Chem. Phys. 159, 224501 (2023); doi: 10.1063/5.0177363
Submitted: 21 September 2023 • Accepted: 7 November 2023 •
Published Online: 8 December 2023

Víctor M. Trejos,[1,2] Marcos de Lucas,[2] Carlos Vega,[2] Samuel Blazquez,[2,a)] and Francisco Gámez[2,a)]

AFFILIATIONS

[1] Departamento de Química, Universidad Autónoma Metropolitana-Iztapalapa, Av. San Rafael Atlixco 186, Col. Vicentina, 09340 Ciudad de México, Mexico
[2] Departamento de Química Física, Universidad Complutense de Madrid, 28040 Madrid, Spain

[a)] **Authors to whom correspondence should be addressed:** samuelbl@ucm.es and frgamez@ucm.es

ABSTRACT

The importance of nitrate and ammonium salts both in the environment and in biological processes cannot be questioned. In this work, using the TIP4P/2005 water model, aqueous solutions of nitrate and ammonium electrolytes are parametrized using scaled charges while keeping a rigid structure and nonpolarizable charge distributions. The models are optimized by systematically testing a set of properties for twelve electrolytes—eight nitrate and four ammonium salts—thus, enlarging the number of potential chemical species encompassed within the Madrid-2019 force field for ions. The capacity of the force field for predicting densities, ion–ion and ion–solvent structures, and transport properties of the solutions comprised by the trial batch of salts was tested and discussed. Both the dependence of the densities with the salt concentration and the solution structure were nicely reproduced by the models in the whole concentration range without any trace of precipitating events and with improved accuracy in comparison with recently reported models, while the agreement of the simulated transport properties with experimental data ranges from good to reasonable, depending on the ion/counterion pair. These scaled charge models might be considered as force fields embodying a reasonable compromise between exactness and general applicability and also as an important step in the development of accurate models for polyatomic ions.

I. INTRODUCTION

Nitrogen is the main component of the atmosphere, but only a small percentage is disposable for its biological fixation in the form of essential amino acids after the action of cosmic rays (to form NO_x) and N_2 reduction to NH_4^+ by the biochemical processes carried out by certain microorganisms (*Rhizobium*, *Azobacter*, *Cyanobacteria,* and *Actinomycetes*), the so-called nitrogen-fixing bacteria. The ammonium fixed in lithosphere is then oxidized in a two-step process termed nitrification: (a) nitrosation, by the *Nitrosomonas*, and (b) a final oxidation to NO_3^-, by the genus *Nitrobacter*. The process is compensated by the reduction (or denitrification) of oxidized species by the *Pseudomonas*. Definitely, both NO_3^- and NH_4^+ play an active role in the nitrogen cycle, one of the most relevant biogeochemical cycles for life and environmental preservation.[1] Both chemical species are of key biological importance, since they are metabolites in a multitude of biochemical pathways of amino acids, such as nitrate assimilation by photosynthetic eukaryotic organisms[2] or the transfer of ammonium in the glutamate cycle.[3] In the case of ammonium, its natural source is the abundant NH_3 gas, one of the few components in the atmosphere with a basic character, which plays a double role from the perspective of global health: It partly alleviates the effects of acid rain provoked by HNO_3 among other acids, but, once dissolved, it is a main component of aerosols in the form of $(NH_4)_2SO_4$ and NH_4NO_3, consequently contributing to climate change.[4] Additional sources of nitrogenated molecules are of anthropogenic nature. From an industrial point of view, nitrate and ammonium salts such as $NaNO_3$, KNO_3, or NH_4NO_3 are widely used in the pharmaceutical and chemical industries.[5] Other sources are emissions from combustion engines and, much more

importantly, fertilizers, whose use, generalized after the discovery of the Haber–Bosch process, allowed for global population growth and initiated, at the time, the acidification of soils and the eutrophication of oceans and sweet-water reservoirs.[6]

To provide with a robust and accurate force field for the most important nitrogenated species, i.e., NO_3^- and NH_4^+ in water environments, two ingredients are logically needed: a versatile force field for water and a recipe for succeeding in the parametrization of ion–ion and ion–solvent interactions. The development of models for water has a long history. The very first attempt of Bernal and Fowler[7] paved the way for the development of TIP models of Jorgensen and co-workers in the 1980s[8,9] and the subsequent polarization-corrected SPC/E model of Berendsen and co-workers.[10] Within this panorama, throughout the years some groups have gathered the most salient features of both model families to generate a new improved set of force fields. From all of them, the TIP4P/2005 stood out for being capable of reproducing a wide variety of water properties, including density, viscosity and diffusion coefficients, surface tension, and even anomalies such as the temperature of the maximum in density.[11]

Concomitant to the development of water models, in recent years many force fields for ions have been reported.[12–34] While most of these models predict hydration-free energies accurately, they failed when dealing with other properties. For instance, some authors[35,36] showed that at high concentrations, all force fields overestimate the decrease in diffusion coefficient of water due to the addition of a soluble salt. In this context, some of us started to develop the so-called Madrid-2019 set of force fields,[37,38] constructed by using a scaled charge of 0.85 electron units, in the spirit of the works by Leontyev and Stuchebrukhov[39–41] to *effectively* account for the solvent screening of the electrostatic interactions. Scaled charge models have also demonstrated to be useful in simulations of biological systems.[42,43] The ion force fields enclosed in the Madrid-2019 model have been employed to successfully study the specific shifts of temperature of maximum in density[44,45] after adding salts to water, the freezing depression of ice,[46] the phase diagram of aqueous solutions of LiCl,[47] the salting out effect of methane in water,[48] the adsorption behavior of electrolytes at interfaces,[49] the three-phase equilibrium of methane hydrate in NaCl solutions,[50] or, very recently, the electrical conductivity of electrolytes,[51] to mention a few.

Since the importance of these two ions (nitrate and amonium) has not gone unnoticed in the field of molecular simulations, several models for both nitrate and ammonium have been reported. Among the nonpolarizable models for the nitrate ion, we highlight the following: (i) flexible or rigid all-atom models used for modeling ionic liquids,[52–55] surfaces,[56] bulk aqueous solutions or solids,[57] all employing a charge distribution based on *ab initio* calculations; (ii) non-charged models based on a Buckingham potential for solutions[58] or molten salts;[59] (iii) a force field family in which the Lennard-Jones–Coulomb potential parameters are derived from a hybrid quantum mechanics–molecular mechanics approach[60] that has been widely employed for exploring the experimental results for the structure of $NaNO_3$ solutions as obtained from x-ray and neutron diffraction or the hydration of $AgNO_3$[61] or nitrate salts[62] such as $NaNO_3$[63] and KNO_3;[64] (iv) transferable and multipurpose rigid models for use in solid and solutions;[65] and, finally, (v) force fields in which the optimization of the van der Waals interaction parameters is sought by employing the hybrid RISM-SCF-SEDD method.[66,67] The most recent report on the simulation of nitrate salts[68] exploited the parameters obtained in the framework of the Self-Consistent Field-Site-Site–Ornstein–Zernike method in Ref. 69 for electrolytes in SPC/E water to optimize a force field where densities, activities, and diffusion coefficients in the dilute regime were selected as target properties.

Surprisingly, the growth of nonpolarizable force fields for NH_4^+ has been comparably limited in the literature. Some examples are those using the *ab initio* restrained electrostatic potential for studying the ion pair dynamics[70] and those handling hybrid methods[71] or Optimized Potentials for Liquid Simulations (OPLS)-like models[72] to provide insight into the crystallization of NH_4Cl,[73] ionic liquid properties,[74] ammonium nitrate solutions,[75] surface properties of ammonium electrolytes,[76] or its hydration-free energies.[72]

Herein, we will develop accurate force fields for both NH_4^+ and NO_3^- in a solution of TIP4P/2005 water as solvent. The potential parameters are optimized with the aid of experimental values of several properties of twelve electrolyte solutions with the goal of enlarging the number of ions in the Madrid-2019 force field by incorporating the optimized interaction parameters for nitrate and ammonium. The models are able to reproduce the curvature of density with the concentration and the structure of solutions in the full concentration range, while exploring the predictions of the transport coefficients paves the way for obtaining hints about how to play with the relationship between the scaled-global charge and the charge distribution in polyatomic ions that might be further studied when developing force fields for chemical species with complex charge densities.

II. SIMULATION DETAILS

Molecular dynamics simulations have been carried out using the GROMACS package[77,78] in the isobaric–isothermal (NpT) and canonical (NVT) ensembles. Unless otherwise mentioned, all simulations were run at 298.15 K and atmospheric pressure (1 bar). We have employed the leap-frog integrator algorithm[79] with a time step of 2 fs. Periodic boundary conditions have been employed in all the xyz directions. The pair potential $u(r_{ij})$ between two atoms (i,j) in different molecules a distance r_{ij} apart can be described as a Lennard-Jones (characterized by a length, σ_{ij}, and energy, ε_{ij}, parameters) and a Coulombic interaction (characterized by the atomic charges, q_i) as follows:

$$u(r_{ij}) = 4\varepsilon_{ij}\left[\left(\frac{\sigma_{ij}}{r_{ij}}\right)^{12} - \left(\frac{\sigma_{ij}}{r_{ij}}\right)^{6}\right] + \frac{1}{4\pi\varepsilon_0}\cdot\frac{q_i q_j}{r_{ij}}, \qquad (2.1)$$

with ε_0 being the vacuum permittivity. The temperature and pressure were kept constant by employing the Nosé–Hoover thermostat[80,81] and the Parrinello–Rahman barostat,[82] respectively, both with time constants of 2 ps. The cutoff radii for both electrostatics and van der Waals interactions were fixed at 10 Å. Analytical long-range corrections were applied to the Lennard-Jones contributions to the energy and pressure. The smooth particle–mesh Ewald method[83] was used to account for the long-range electrostatic forces. The interaction parameters for the counterions (i.e., halogen anions and SO_4^{2-} for NH_4^+ and alkali ions and Mg^{2+} and Ca^{2+} for

NO_3^-) were obtained from the Madrid-2019 force field,[37,38] while those of the TIP4P/2005 model are set according to Ref. 84. The geometrical constraints of these polyatomic ions were maintained using the LINCS algorithm[85,86] for nitrate salts and the SHAKE algorithm[87] for electrolytes containing ammonium or sulfate ions.

The force field was developed as follows. The atomic charges describing the Coulombic part of the pair interaction of NH_4^+ were selected from the OPLS-based model derived in Ref. 88 for the study of ion hydration, while those NO_3^- were obtained from Refs. 52 and 53, in which the charges were obtained by fitting the gas-phase potential energy surfaces derived from high-level quantum chemical calculations and employed for exploring the thermodynamics of ionic liquids. These charges were afterward scaled by a factor 0.85 in our approach. The LJ parameter ε_{ii} was also obtained from these references, but, for simplicity, σ_{ii} was fixed to 3.15 Å for both the nitrogen atoms in the ammonium and nitrate ions. The geometry of the NO_3^- and NH_4^+ models were set from Ref. 75 and collected in the caption of Table I. Those parameters defining the cross-interaction between the atoms of the nitrate with those of the ammonium group, and the interactions of the nitrate and ammonium groups with their counterions (σ_{ij} and ε_{ij}) were fitted by optimizing the match between simulated and experimental data of a selected set of experimental properties without assuming the Lorentz–Berthelot (LB) or other combination rule, following Refs. 37 and 38. The optimized potential parameters are collected in the *topology* file for GROMACS provided as supplementary material and also in Tables I and II, Tables S1 and S2. Particularly, in Table I we present the pair potential parameters for the nitrate–nitrate and ammonium–ammonium interactions, while in Table II the ion–counterion interactions are described. In Table II, we omitted the numerical values of those interactions for which they were set to the value obtained with the LB rule. The whole set of numerical values are provided in S1 and S2. To avoid confusion, the O and H atoms of water are indicated by a subscript *w*, O atoms from sulfate group by a subscript *s*, those atoms belonging to ammonium with a subscript *a* and, finally, those of nitrate are marked with a subscript *n*.

TABLE I. Summary of the force field parameters for the Lennard-Jones (σ_{ii}, ε_{ii}) and Coulombic (atomic charges, q_i) contributions to the pair potential for nitrate and ammonium ions, as developed in this work. The atomic charges were extracted from Ref. 88 for NH_4^+ and Refs. 52 and 53 for NO_3^- and later scaled to a global charge of $\pm 0.85e$. The LJ parameters (σ_{ii} and ε_{ii}) were mainly obtained from Refs. 52, 53, 88 and 75, but σ_{ii} for both the nitrogen atoms in the ammonium and nitrate ions is fixed to 3.15 Å. The geometry of the NO_3^- ion is defined by a $\widehat{ONO}$ angle of 120° and a O_n–N_n bond distance of 1.256 Å. Similarly, for NH_4^+ the $\widehat{HNH}$ angle is 109.5°, and the N_a–H_a bond distance is 1.010 Å. See Fig. S4 for a schematic model of these ions and Table II, Tables S1 and S2 for the numerical parameters defining the interactions between NO_3^-, NH_4^+, water, and counterions.

NO_3^-	σ_{ii} (Å)	ε_{ii} (kJ mol^{-1})	q_i (e)
N_n	3.15	0.711	+0.6749
O_n	2.86	0.878	−0.5083
NH_4^+	σ_{ii} (Å)	ε_{ii} (kJ mol^{-1})	q_i (e)
N_a	3.15	0.711	−0.3400
H_a	0.00	0.000	+0.2975

TABLE II. Lennard-Jones σ_{ij} parameters (in Å) between nitrate, ammonium, and the counterions. Notice that σ_{H_a} is zero and, consequently, not included in the table. Parameters for TIP4P/2005 water were taken from Ref. 84. LJ parameters for the self- and cross-interaction between Li^+, Na^+, K^+, Rb^+, Cs^+, Mg^{2+}, Ca^{2+}, F^-, Cl^-, Br^-, SO_4^{2-}, and water are taken from the Madrid-2019 force field.[37,38] In cases where a numerical value is not provided, we suggest to use the LB combination rules for the description of multielectrolyte solutions. LB (boldface) means that LB rules were used and tested against experimental data for binary solutions. The LB rule was always followed for the ε_{ij} parameter. See Tables S1 and S2 in the supplementary material for specific numerical values. The sulfate ion is split into S and O_S moieties.

Atom	N_n	O_n	N_a
O_w	**LB**	3.23	3.054
Li^+	**LB**	3.30	LB
Na^+	**LB**	3.00	LB
K^+	**LB**	3.30	LB
Rb^+	**LB**	3.20	LB
Cs^+	**LB**	3.40	LB
Mg^{2+}	**LB**	3.40	LB
Ca^{2+}	**LB**	2.76	LB
N_a	3.90	**LB**	a
F^-	LB	LB	3.54
Cl^-	LB	LB	**LB**
Br^-	LB	LB	**LB**
N_n	a	**LB**	3.90
O_n	**LB**	a	**LB**
S	LB	LB	**LB**
O_S	LB	LB	3.30

[a]These values are reported in Table I.

During the simulations, bulk densities (ρ) and radial distribution functions [$g(r)$ or RDFs] were obtained by the appropriate average over the trajectories generated in NpT simulations of boxes comprised by 555 water molecules and the corresponding number of ions needed to achieve the desired molality (i.e., the number of moles of salt per kilogram of water) over ~50 ns. Statistical uncertainties in ρ amounts to 0.25%. The hydration number (HN) and the number of contact ion pairs (CIPs) are evaluated from the corresponding RDF. For instance, the cation–anion CIP ($CIP_\pm$) is defined as follows:

$$CIP_\pm = 4\pi\rho_\pm \int_0^{r_{\min}} g_\pm(r) r^2 dr, \tag{2.2}$$

where $g_\pm(r)$ is the cation–anion RDF, $r_{\min}$ the position of the first minimum of the integrated RDF, and $\rho_\pm$ the lower number density after dissociation (i.e., in a salt of the type MX_2 it would be the number density of the cation, M, while in a salt with stoichiometry M_2X, $\rho_\pm$ equals the number density of the anion, X). Details about how to distinguish CIP and solvent-separated ion pairs will be provided below. As it will be shown, the nitrogen–nitrogen CIP_N is also key in explaining the structural features of nitrates. It will be defined as

$$CIP_N = 4\pi\rho_N \int_0^{r_{\min}} g_{N-N}(r) r^2 dr, \tag{2.3}$$

TABLE III. Experimental salt solubility in water at 298.15 K and 1 bar in molality units as reported in Ref. 89.

Salt	Solubility (mol kg^{-1})
$LiNO_3$	14.8
$NaNO_3$	10.7
KNO_3	3.8
$RbNO_3$	4.4
$CsNO_3$	1.4
$Mg(NO_3)_2$	4.8
$Ca(NO_3)_2$	8.8
NH_4F	22.5
NH_4Cl	7.4
NH_4Br	8.0
NH_4NO_3	26.6
$(NH_4)_2SO_4$	5.8

where ρ_N is the number density of the nitrogenated ion and $g_{N-N}(r)$ the nitrogen–nitrogen RDF. Finally,

$$HN = 4\pi\rho_w \int_0^{r_{\min}} g_{(\pm)-O_w}(r) r^2 dr, \tag{2.4}$$

where ρ_w is the number density of water and $g_{(\pm)-O_w}$ the cation/anion–O_w RDF. For the polyatomic ions optimized here, the RDF is taken by considering the central nitrogen atom.

A bigger system with 4440 water molecules was simulated also for 50 ns in the *NVT* ensemble for visually evaluating the absence of precipitation of the salts close to the experimental solubility limit. The experimental values of the solubility limits at 25 °C are shown in Table III for the sake of completeness. Cells of the same size were also employed for computing the diffusion, D, and shear viscosity, η, coefficients. Briefly, we performed a preliminary NpT simulation of 20 ns to calculate an average box volume V. After that, a NVT simulation of 50 ns with a pressure tensor $P_{\alpha\beta}(t)$ was saved on disk every 2 fs. The shear viscosity was evaluated following the recipe of Gonzalez and Abascal for rigid models[90] via the self-correlation function of the five translational and rotational invariants constructed from the $P_{\alpha\beta}(t)$ components, as formulated in the Green–Kubo formalism,

$$\eta = \frac{V}{kT} \int_0^\infty \langle P_{\alpha\beta}(t)\, P_{\alpha\beta}(0) \rangle\, dt, \tag{2.5}$$

with k being the Boltzmann constant. For the diffusion coefficients, D, we used the Einstein relation,

$$D = \lim_{t\to\infty} \frac{1}{6t} \left\langle [\mathbf{r}_i(t) - \mathbf{r}_i(0)]^2 \right\rangle, \tag{2.6}$$

where $\mathbf{r}_i(t)$ and $\mathbf{r}_i(0)$ are the position of the ith particle at time t and at a certain origin of time, respectively, and $\langle\cdot\rangle$ is the average. The diffusion coefficients were then obtained, avoiding the subdiffusive regime, from the slope of the plot of the mean square displacement (MSD), given by $\langle [\mathbf{r}_i(t) - \mathbf{r}_i(0)]^2 \rangle$, against time. The so-obtained values of D were subsequently modified with the hydrodynamic correction of Yeh and Hummer,[91]

$$D_{corr} = D + \xi \frac{kT}{6\pi\eta L}, \tag{2.7}$$

where D_{corr} is the corrected diffusion coefficient, $\xi = 2.837$, η is the simulated viscosity at the studied concentration, and L is the length of the simulation box.

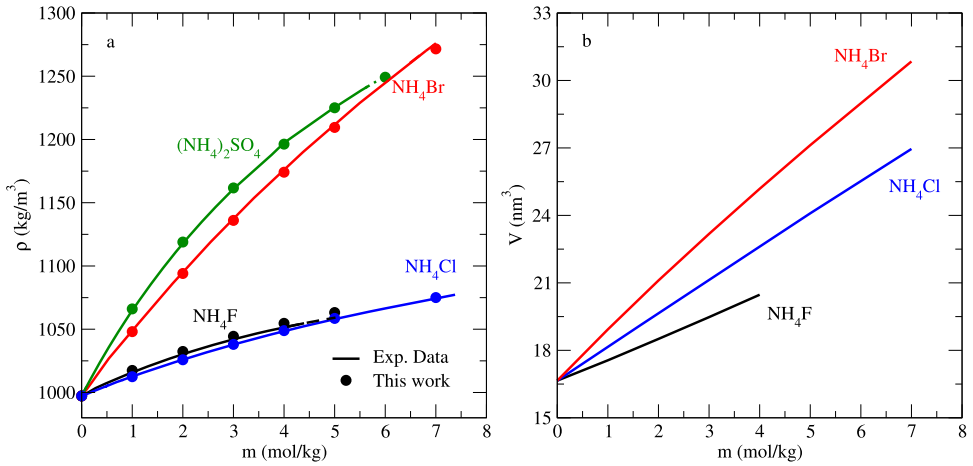

FIG. 1. Density as a function of the molality for aqueous solutions of different ammonium salts. (a) NH_4F, NH_4Cl, NH_4Br, and $(NH_4)_2SO_4$. For NH_4F, both the experimental and simulated data correspond to $T = 291.15$ K. Molecular Dynamics results are represented as full circles and the experimental data are shown as a continuous line. Experimental data for NH_4SO_4 and NH_4Cl were obtained from Refs. 92–94 and for NH_4F and NH_4Br they were extracted from Ref. 95. In the cases where experimental data covered a concentration range below the solubility limit, they have been extrapolated with a cubic spline (dashed lines). (b) Volume occupied by a solution comprised by 555 water molecules as obtained from experimental densities of monovalent ammonium salts as a function of m. See text for details.

III. RESULTS AND DISCUSSION

A. Bulk densities

Figure 1(a) shows the Molecular Dynamics simulation results for the bulk density of the set of ammonium salts considered in this work, i.e., NH_4F, NH_4Cl, NH_4Br, and $(NH_4)_2SO_4$ as a function of molality up to their experimental solubility limit, except for NH_4F, for which the experimental density data are scarce. For all these salts, this is, to the best of our knowledge, the first time that the change of density with concentration is predicted with molecular simulations. In the case of monovalent salts (NH_4F, NH_4Cl, and NH_4Br), we observed a remarkable agreement between the experimental data (solid lines) and the results obtained from simulations (filled circles), with deviations of ~0.4% at most in the whole molality range. The results for each salt are shown in individual graphs (Fig. S1) and tabulated in the supplementary material. Since mass densities are not too useful to describe physical changes (as they are affected by the precise values of the atomic masses), mass dependencies of the density curves are bypassed to assess the volume effect of the anion size in the observed trend for monovalent salts. To that aim, in Fig. 1(b) the volume occupied by a solution comprised by 555 molecules of water at a given molality is presented as obtained from experimental densities. The volume of the solutions increases with the molality and with the anion size at a given concentration. Hence, the fact that the experimental curves do not follow a trend according to the ionic size of the counterions (the densities of NH_4F and NH_4Cl being slightly inverted) indicates a mass effect rather than a shrinking of the solution. For the divalent salt $(NH_4)_2SO_4$, the predicted density and the experimental data are also in good agreement in the whole range of densities until their solubility limit. The relative percentage deviations are generally below 0.1% (see Table SVI of the supplementary material).

In Fig. 2, we show a comparison between the experimental densities of the selected nitrate salts and Molecular Dynamics simulation

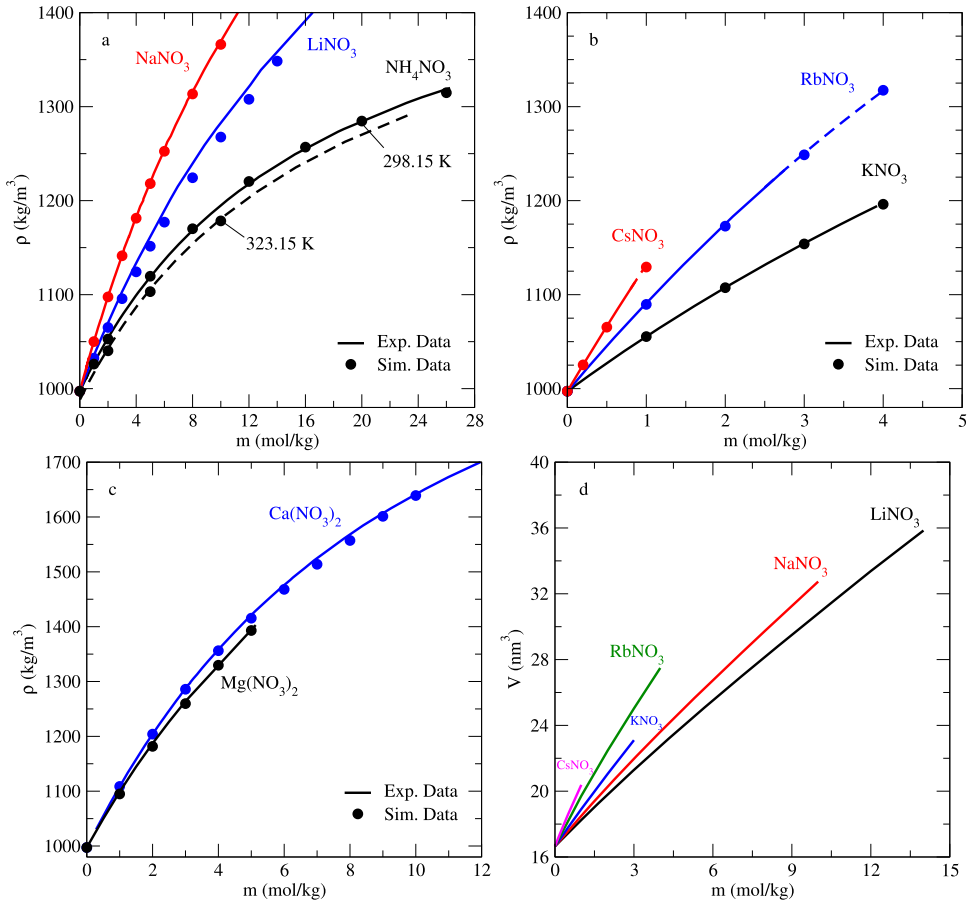

FIG. 2. Density as a function of the molality for aqueous solutions of different nitrate salts. (a) Highly soluble $LiNO_3$, $NaNO_3$, and NH_4NO_3 salts. For the latter, data at 323.15 K are also included. (b) Intermediate-to-poorly soluble KNO_3, $RbNO_3$, and $CsNO_3$ salts. (c) Divalent $Mg(NO_3)_2$ and $Ca(NO_3)_2$ salts. The Molecular Dynamics results are shown with filled circles, while continuous lines stand for the experimental data, except for NH_4NO_3 at 323 K where experimental results are shown as a black dashed line. The experimental data are obtained for most salts from Refs. 92–94, but the experimental information for $RbNO_3$ and $CsNO_3$ were extracted from Refs. 96 and 97, respectively. In the cases where experimental data covered a concentration range below the solubility limit, they have been extrapolated with a cubic spline (see dashed red and blue lines for $CsNO_3$ and $RbNO_3$, respectively). (d) Volume occupied by a solution comprised by 555 water molecules as obtained from experimental densities of alkaline nitrates as a function of *m*. See text for details.

results. This comparison is done for concentrations up to the experimental solubility limit, as in the previous cases. We have developed a force field for eight different salts, including the combination with the NH_4^+ cation previously optimized. The nitrate salts are formed combining the NO_3^- anion with the cations of the Madrid-2019 force field and its extended version[37,38] (i.e., Li^+, Na^+, K^+, Rb^+, Cs^+, Mg^{2+}, and Ca^{2+}). As can be seen in Fig. 2, the agreement between experimental and Molecular Dynamics simulation data, even for the highly soluble salts, is remarkable in the whole concentration range and in better agreement with experiments than those reported in Refs. 68 and 75. A detailed comparison with those simulation data is provided in the supplementary material (see Figs. S2 and S3), where the plots of the bulk density against molality for each salt are individually shown in comparison with literature data. Particularly, in Fig. 2(a) we show the density results for the highly soluble $LiNO_3$, $NaNO_3$, and NH_4NO_3 electrolytes. The predicted density for $NaNO_3$ and NH_4NO_3 closely matches the experimental data with deviations generally below 0.3%. The NH_4NO_3 salt deserves special attention, as it constitutes a nice test for both NH_4^+ and NO_3^- force fields. For that reason, in Fig. 2(a) we have incorporated simulation data at 323.23 K in comparison with experimental information as an additional confirmation of the performance/transferability of the new force field when working at temperatures different from those for which it has been optimized. In this case, the Molecular Dynamics simulation results accurately reproduce the experimental densities of NH_4NO_3 up to a concentration of 26 *m* at 298.15 K and are in better agreement than those recently reported in Ref. 98. At a higher temperature, the agreement is identically remarkable as observed in Fig. 2(a). The densities of $CsNO_3$, $RbNO_3$, and KNO_3 are shown in Fig. 2(b). We observed that the predictions are also in good agreement with the experimental data for all three cases with deviations below ~0.25% for all salt concentrations. Identically, in Fig. 2(c) we provide satisfactory predictions for the divalent salts $Mg(NO_3)_2$, and $Ca(NO_3)_2$, which are often considered more challenging to be modeled.

In Fig. 2(d), we also plot the volume occupied by 555-water molecules solution. The volumes increase with the counterion size, as previously described for ammonium salts. This result is discordant with those found from simulation (see Refs. 44, 45 and 99 and references therein), where it was found that the ordered hydration shell of Li^+ is responsible for a solution expansion, and indicates that the NO_3^-–solvent interaction strongly competes with the expanding effect arising from the cation–water coordination.

Overall, the extension of the Madrid-2019 force field for nitrate and ammonium salts presented here provides satisfactory predictions compared with experimental data for densities in the entire molality range. In the following sections, the computed structural and transport properties of nitrate and ammonium electrolyte solutions are tested against experiments to further prove the accuracy and reliability of the proposed force fields.

B. Ion coordination and radial distribution functions

The nonspherical symmetry of polyatomic cations NH_4^+ and NO_3^- and their H-bonding features in water environments entail a complex hydration scenario that hampers the collation among experimental data and computational results, since the coordination of the ions is studied by means of RDFs, that seems not to be best selection among the pair distribution functions not only because their anisotropic geometry but for the occurrence of three-body arrangement.[100] In this section, the relevant features of the ion–ion and ion–water structure are discussed in the light of the dispersed data found in the literature. For the sake of discussion, in Fig. S5 we present the simplified structure of the ion-counterion structure of either CIP or solvent-separated ion-pair (SSIP) arrangements, together with the RDFs pattern expected for such molecular distributions for all the potential cases, i.e., (a) NH_4X (ammonium and atomic anion, X), (b) MNO_3 (nitrate and atomic cation, M), and (c) $NH_4NO_3/(NH_4)_2SO_4$ (polyatomic anion and cation). In (a), the existence of $CIP_\pm$ can be verified by the partial overlap of the $N_a\cdots X$ and $N_a\cdots O_w$ RDFs, while the $N_a\cdots X$ RDF is separated from RDFs related with the ammonium or X hydration in the SSIP arrangement. If the structure of MNO_3 presents CIP then the $N_n\cdots M$ and $N_n\cdots O_w$ RDFs overlap, at least partly, while the maximum of the $N_n\cdots M$ RDF is shifted to higher distances in the SSIP configuration. Finally, in the polyatomic cases considered here, the anion–cation structure by a RDFs pattern in which the RDFs of interest are clearly distinguishable because solvation water precludes the intermolecular proton–bond between the nitrogenated ions.

We shall start the discussion with the nitrate ion. NO_3^- has a planar D_{3h} geometry that allows the coordination with water to be possible in both radial and axial directions. This fact leads to a complex situation in which the ion–water interaction might be partly feeble and distorted. There are many simulations and experimental data on the coordination of nitrate, but some are at odds between them. Infrared spectroscopy suggests that the nitrate group is coordinated with four molecules of water.[102] However, the analysis of neutron diffraction data rather suggests a pentacoordination of the nitrate group with water,[103] with ~1 molecule in the axial position, at distances of $N_n\cdots H_w$ ~ 2.05 Å and $N_n\cdots O_w$ ~ 2.65 Å on average, and the remaining at $N_n\cdots O_w$ ~ 3.4 Å. Such distinct water arrangements around a nitrate ion are observed in the simulated $N_n\cdots O_w$ RDF as a double peak: The first corresponds to direct or axial $N_n\cdots O_w$ interactions, while the second (describing molecules of water in the direction of the nitrate plane) is the indirect N_n–$O_n\cdots H$–O_w coordination. However, the $N_n\cdots O_w$ distance of the axial water obtained from the simulations is not in agreement with the experiments. X-ray scattering of NH_4NO_3 solutions[104] determined the $O_n\cdots H_w$ distance to be 2.885 Å, while a value of ~3.5 Å is proposed for the $N_n\cdots O_w$ distance. Most reliable data are those obtained from time-of-flight neutron diffraction of $NaNO_3$ solutions,[105]leading to a pentacoordination scenario with a $N_n\cdots H_w$ distance of 2.80 Å and of 3.8 Å for that of the $N_n\cdots O_w$ pair.[104,105] In fact, more recent wide-angle x-ray scattering experiments on aqueous KNO_3 confirmed a $N_n\cdots O_w$ distance of 3.63 Å[106] and a decacoordinated structure, in agreement with the results previously established in the work of Megyes *et al.*[63] using x-rays and neutron diffraction of aqueous $NaNO_3$ solutions. Older data on x-ray diffraction on $Zn(NO_3)_2$ solutions lead to a coordination value of ~18.[107] All these results are in sharp contrast with the value of 0.5 obtained with NMR experiment data presented in Ref. 108. Neutron diffraction data from Ref. 109 lead to values in the range 15–20. Simulation values of the first maxima of the $N_n\cdots O_w$ RDF range from the 3.4–3.5 Å provided by polarizable models,[110,111] the 3.65 Å calculated with *ab initio* Molecular Dynamics[112] or the 3.68 Å obtained within the RISM-SCF

method.[113] Classical simulations employing nonpolarizable models lead to $N_n \cdots O_w$ distances of 3.5 Å for rigid[114] and 3 48 Å for flexible models,[75] respectively. However, the coordination number of nitrate in aqueous solution obtained from computational methods spans values from 6 to 20.[63,115–117] Within this complex panorama, our models predicted roughly constant values for the peaks of the $N_n \cdots H_w$ and $N_n \cdots O_w$ RDFs of ~2.8–3.0 and 3.6–3.7 Å respectivel, which are in very nice agreement with both the previous simulation results and experimental data within the uncertainties reported in the literature. In this work, the calculated HN_N values fall between 15 and 20 for all the nitrate salts. Taking into account the variability of experimental measurements, our results are reconcilable with those experiments that can be considered reliable. The particular case of NH_4NO_3 has been recently studied employing classical and *ab initio* Molecular Dynamics study.[98] They demonstrated that at 0.05 *m* dilution, NH_4^+ hydration involves around 6 water molecules, while at an increased concentration of 11 *m*, the hydration number drops to ~3.6. Interestingly, our results at 26 *m* exhibit a similar trend, with ~3 water molecules surrounding NH_4^+ (see Table IV where all structural results of this work are presented). Turning to the hydration of NO_3^- in this electrolyte, authors of the work of Patil *et al.* reported smaller hydration in comparison with alkali nitrates, with HN_N ~ 10.5 for substantially diluted solutions and ~7 for more concentrated ones. Our findings similarly indicate a higher hydration number of the nitrate anion compared to the ammonium cation, but with a notably larger hydration number of 12, both ions being substantially less hydrated in comparison with solutions in which they are present with atomic (alkali or halogen) counterions (see below for NH_4^+). This said, it becomes apparent that the difference between the homogeneous structure obtained for alkali nitrates and ammonium nitrate hides a few specific relations on the nuanced hydration dynamics of the nitrate and ammonium ions that are unexpectedly well grasped by the Molecular Dynamics study performed within the proposed force field.

TABLE IV. Structural properties for nitrate and ammonium electrolyte solutions both at the lowest molality considered and in the solubility limit of each salt. The selected features are the ion–counterion structure (i.e., CIP or SSIP), the values of $CIP_\pm$ (i.e., cation and anion contacts) and CIP_N (nitrate–nitrate or ammonium–ammonium contacts), the hydration numbers of the nitrate or ammonium ion (HN_N), or of the counterion (HN_{CI}), and the position of the first maximum of the nitrogen–O_w ($d_{N\cdots O_w}$), nitrogen–water hydrogen ($d_{N\cdots H_w}$), and the counterion–water oxygen ($d_{CI\cdots O_w}$) in the corresponding radial distribution functions. In the case of NH_4NO_3, the ammonium is considered to be the counterion. For nitrates, the cation-O_n RDF is selected to evaluate the CIPs. In the latter case, a factor of three must be included to account for the three O_n atoms of the nitrate ion. The value of $\delta = d_{O_w\cdots O_w} - 0.5 \cdot (d_{N\cdots O_w} + d_{CI\cdots O_w})$, as defined in Ref. 101, is also included. Note that the distance $d_{O_w\cdots O_w}$ is 2.80 Å. The molality is given in units of mol/kg and distances in Å. We include a line for each parametrized ion in which we collect the experimental interval for HN_N, $d_{N\cdots O_w}$ and $d_{N\cdots H_w}$, when available. Discussion about the counterion–water structures can be found in Refs. 37 and 38. Notice that a rigurous calculation of the $CIP_\pm$ in the case of nitrates would require a specific evaluation of the spatial distribution of the cation around the nitrate anion to account for both axial and in-plane ion-counterion interactions.

Salt	*m*	Cation–Anion structure	$CIP_\pm$	CIP_N	HN_N	HN_{CI}	$d_{N\cdots O_w}$	$d_{N\cdots H_w}$	$d_{CI\cdots O_w}$	δ
$LiNO_3$	1	SSIP	0	0.3	24.5	4.0	3.66	2.82	1.84	0.05
	14	SSIP	0	3.7	14.0	4.0	3.61	2.81	1.83	0.08
$NaNO_3$	1	CIP	0.1	0.3	20.9	5.5	3.68	2.81	2.34	−0.21
	10	CIP	0.6	2.8	14.6	5.2	3.61	2.87	2.32	−0.17
KNO_3	1	CIP	0.2	0.2	24.0	6.7	3.62	2.80	2.74	−0.38
	4	CIP	0.7	1.2	18.9	6.5	3.63	2.79	2.73	−0.38
$RbNO_3$	1	CIP	0.9	0.6	20.9	5.7	3.58	2.80	2.74	−0.36
	4	CIP	2.3	2.1	16.2	4.6	3.68	2.76	2.74	−0.41
$CsNO_3$	0.2	CIP	0.5	0.0	26.0	6.5	3.69	2.71	2.84	−0.47
	1	CIP	0.7	0.4	22.3	6.1	3.65	2.73	2.86	−0.46
$Mg(NO_3)_2$	1	SSIP	0	0.2	20.2	6.0	3.66	2.79	1.93	0.01
	5	SSIP	0	3.2	14.2	6.0	3.60	2.78	1.91	0.04
$Ca(NO_3)_2$	1	CIP	0.9	0.7	20.9	7.5	3.63	2.74	2.41	−0.22
	10	CIP	1.3	5.2	10.1	4.9	3.65	2.94	2.39	−0.22
NH_4NO_3	1	CIP	0.5	0.3	22.0	5.6	3.67	2.76	2.65	−0.36
	26	CIP	3.8	4.3	9.7	3.0	3.58	2.74	2.66	−0.32
NO_3^-(expt.)	···	···	···	···	[5–20]	···	[2.65–3.8]	[2.05–2.9]	···	···
NH_4F	1	CIP	0.2	0	5.4	5.4	2.65	3.18	2.76	0.10
	5	CIP	0.7	0	4.7	4.8	2.66	3.18	2.77	0.09
NH_4Cl	1	SSIP	0	0	5.5	5.8	2.66	3.22	3.05	−0.06
	7	CIP	0.1	0	5.3	5.6	2.65	3.20	3.04	−0.05
NH_4Br	1	SSIP	0	0	5.6	6.2	2.66	3.22	3.14	−0.10
	7	CIP	0.1	0	5.2	5.6	2.66	3.20	3.15	−0.11
$(NH_4)_2SO_4$	1	CIP	0.4	0	5.2	7.7	2.64	3.18	3.76	−0.40
	6	CIP	1.0	0	4.1	5.3	2.68	3.16	3.75	−0.42
NH_4^+(expt.)	···	···	···	···	[4–5]	···	[2.91–3.06]	···	···	···

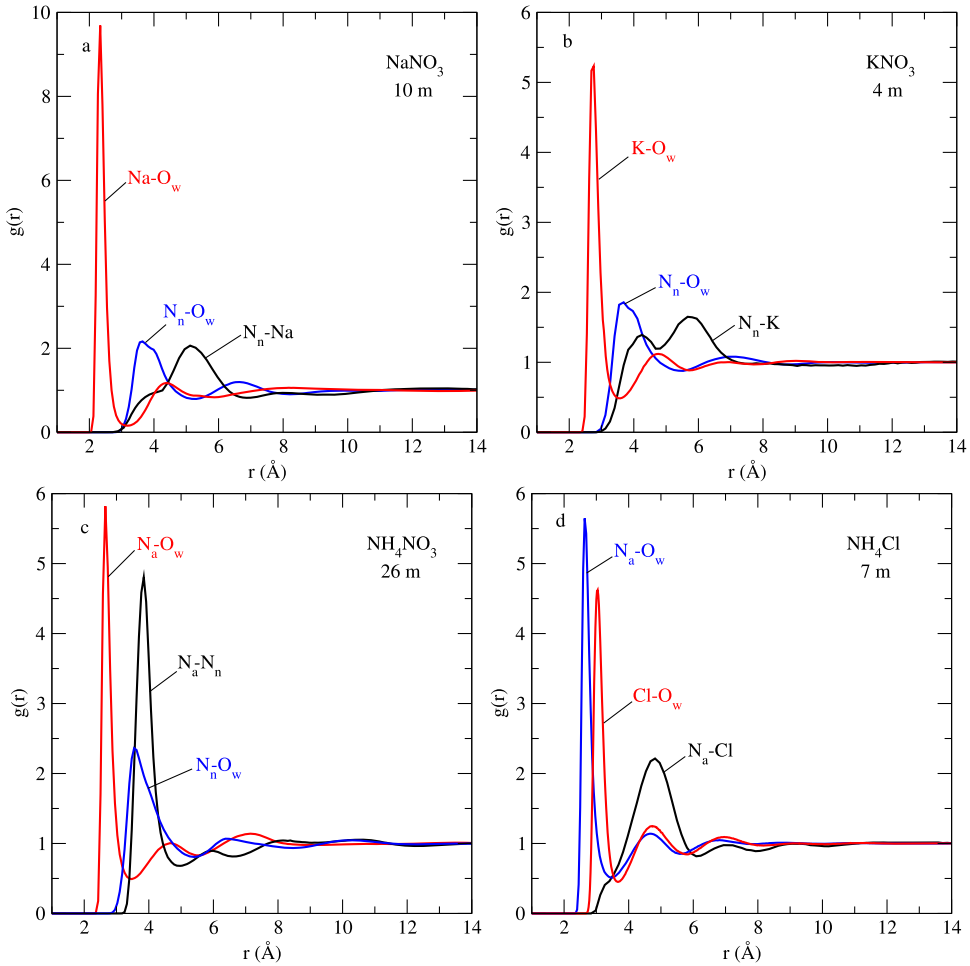

FIG. 3. N_n or N_a–counterion (black), N_n or N_a-O_w (blue) and counterion–O_w (red) radial distribution functions for (a) $NaNO_3$ 10 *m*, (b) KNO_3 4 *m*, (c) NH_4NO_3 26 *m*, and (d) NH_4Cl 7 *m* electrolyte solutions. In the case of NH_4NO_3, the ammonium is considered to be the counterion.

In relation with the ion-counterion structure the three RDFs of interest are not overlapping for $LiNO_3$ and $NaNO_3$ as shown in Fig. 3(a) for $NaNO_3$. Identically, this is the RDF pattern for $Mg(NO_3)_2$. From the 3D models and the scheme of the RDFs shown in Fig. S5, the ion-counterion structure of $LiNO_3$ and $Mg(NO_3)_2$ is predominantly of the SSIP type, although some $CIP_\pm$ are observed in $NaNO_3$. With increase in the counterion size, the solubility diminishes (although non-monotonously) and, hence, a CIP structure with an appreciable value of the $CIP_\pm$ number is expected. This is the case of $RbNO_3$, $CsNO_3$, and also for the soluble $Ca(NO_3)_2$ and NH_4NO_3 salts. KNO_3 can be considered a salt with a SSIP-to-CIP transition structure, as can be seen in the double peak in the $N_n \cdots K^+$ RDF in Fig. 3(b). Similarly, the RDFs of NH_4NO_3 also display a CIP structure [see Fig. 3(c)]. The presence or absence of $CIP_\pm$ can be verified by examining the behavior of HN_{CI}: When $CIP_\pm$ are present, they increase with concentration, thus reducing the value of HN_{CI} because the hydration water within the first hydration shell is partly substituted by counterions. Consequently, a marked decrease in HN_{CI} as the salt concentration increases, as seen for instance in NH_4NO_3 or $RbNO_3$, indicates a substantial presence of $CIP_\pm$ at elevated concentrations, as confirmed from the RDFs. Interestingly, the strong dependence of HN_N with concentration is apparent and surprising but might explain the heterogeneous experimental data found in the literature. The structural features indicated that nitrate–nitrate contact ion pairs are present in a T-shape configuration sustained by electrostatic $N_n \cdots O_w$ interactions and, consequently, the CIP_N number increases with the salt molality. Such clustering has been previously observed by Molecular Dynamics in relation with the conductivity of $NaNO_3$ in aqueous solutions.[118] In Fig. S9, we report the N_n–N_n RDF and N_n–O_w RDF for $LiNO_3$ 14 *m*, as an example of this dimerizing effect. Moreover, in Table IV the CIP_N is shown in order to provide a quantitative measurement of this salient feature. A difference of one order of magnitude between the limits of the considered concentration range is observed in all cases. Since the direct effect of such arrangements is of excluded volume nature, the diminution of HN_N with *m* is quickly understood. The presence of $CIP_\pm$ in some salts contributes to the decrease in HN_N as well. The remaining question is whether the incorporation of the dimer structures into the molecular

models employed to deconvolute and interpret the structure factor obtained in diffraction experiments might clarify the entangled panorama related with the structure (either coordination or hydration) of aqueous nitrate solutions.

We close the section with the results for the *quasi*-spherical ammonium ion. While the NH_4^+ ion is of simple tetrahedral geometry (point group T_d), their hydration geometry is still under scrutiny. Seminal classical Molecular Dynamics simulations of NH_4Cl solutions established a coordination of distinctly oriented 8 water molecules located at a $N_a \cdots O_w$ distance of ~3.05 Å.[119] In contrast, some *ab initio*[120] and classical[121] Molecular Dynamics simulations lead to a coordination number of 5 water molecules (one of them not strongly bonded), while recent first principles *ab initio* Molecular Dynamics employing accurate functionals, classical Molecular Dynamics,[122,123] and quantum Monte Carlo calculations[124] show an hexacoordinated structure sustained in a weak and bifurcated hydrogen bond network. A contrasting value of 13 water molecules per NH_4^+ based on purely *ab initio* calculation has also been reported.[125] The two main sets of experimental data on the structure of NH_4^+ in water also lead to disparate results. The x-ray scattering for NH_4Cl solutions[123] established a position of 3.06 Å for the first maximum in the $N_a \cdots O_w$ component of the structure factor. More reliable experiments come from the neutron diffraction data of a 5 *m* aqueous solution of ND_4Cl provided in Ref. 126 that established that the number of waters in the first hydration shell is 4, and the number of water molecules within the first two hydration shell of ammonium is around 10. The deconvolution of the structure factor leads to a first maximum of the $N_a \cdots O_w$ RDF at ~2.8 Å, in nice agreement with more recent soft-x-ray spectroscopy[121] and a few Molecular Dynamics[75] and Monte Carlo[72] simulation results. Additional information obtained also from x-ray scattering on ammonium halide salts[127] determined that the average water–anion distance is 3.2 Å for the chloride and 3.3 Å for the bromide solutions, with an average $N_a \cdots O_w$ distance of 2.91 Å. The coordination number in these experiments was determined to be ~5. Thus, after taking all the reported information with caution, our simulation results (collected in Table IV predict a roughly constant value of ~2.7 Å for the first maximum in the $N_a \cdots O_w$ RDF i.e., the location of the first coordination shell is slightly underestimated by ~0.1–0.2 Å in comparison with experimental and numerical results in Ref. 126, and also is the counterion$\cdots O_w$ distance, but finding that the average predicted value of $HN_N \sim 5.25$ nicely match the most confident experiments.

Finally, in Fig. 3(d) we present the $N_a \cdots O_w$, $Cl \cdots O_w$ $N_a \cdots Cl$ RDFs for NH_4Cl. Similar behavior is observed for NH_4Br (see the supplementary material). In both cases, we observed that the peak of the $N_a \cdots X$ RDF is located far from the $N_a \cdots O_w$ and $X \cdots O_w$ RDFs. According to the schematic representation of Fig. S5, the ion–ion structure in these electrolytes should be of the SSIP type (see the supplementary material), but some CIP± are observed. However, the peaks of the three RDFs overlap with each other in the NH_4F solution, thus forming a $CIP_\pm$ that is calculated to be about 0.5 on average. A similar structure is found for the divalent $(NH_4)_2SO_4$. However, no CIP_N were found in these salts. The link between the relatively more homogeneous experimental data and the absence of nitrogen–nitrogen contacts in the solutions seems to be direct and coherent.

C. Transport coefficients

1. Viscosities

After studying densities and structural features, the estimation of the shear viscosity is a robust test for the performance of a force field, especially because there are precise experimental data that allow a straightforward comparison with simulations. However, since its evaluation is computationally expensive, we selected seven representative cases to discuss. Particularly, we calculated the viscosities of the moderately to highly soluble nitrate salts $NaNO_3$ and NH_4NO_3, the common and moderately soluble NH_4Cl and KNO_3, the divalent $(NH_4)_2SO_4$ and, finally, we assessed $RbNO_3$ and $CsNO_3$ as benchmarks to evaluate larger polarizable cations.

Recent studies demonstrate that, for monoatomic ions, the viscosities (along with other transport properties such as diffusion coefficients or electrical conductivities) are accurately captured by employing a force field with a net ion charge of $q = \pm 0.75e$[51,128,129] (the so-called Madrid-Transport model). However, although in principle one may expect that a global charge of $\pm 0.85e$ might result in a comparatively poorer agreement with experimental data, it is important to note that during the development of the Madrid-2019 force fields,[37] the outcomes for polyatomic anions, such as SO_4^{2-}, differed from those of atomic species. In such cases, the simulated viscosities underestimated the experimental results, in contrast to alkali, alkaline-earth metals, or halogenated salts of 1:1 stoichiometry. In this context, authors of the work of Habibi *et al.*[130] recently developed a force field for $B(OH)_4^-$, providing a better description of transport properties when dressing the anion with a net charge of $\pm 0.85e$. These observations suggest that the charge distribution within these polyatomic anions (in addition to the value of the net charge of the polyatomic ion) can play a crucial role in the transport coefficients of these salts.

Moreover, the relationship between viscosity and structure might be briefly discussed. Intuitively, shear viscosity in aqueous solutions is expected to be strongly mediated by the ion–water interactions and the potential ability to disrupt the hydrogen bond network established in the solution. This assumption is, in fact, featured in some phenomenological models as the classical Jones–Dole model[131,132] in a first attempt to rationalize the parabolic-like behavior of the viscosity with the concentration of some salts. Briefly, it is implicit in the model that while the solvent–ion interaction is very specific and dominates in the low concentration regime, from a certain concentration on, viscosities always increase because the purely electrostatic ion–ion interactions (or Falkenhagen contribution) surpassed the ion–solvent contribution. Another more recent and successful model is the multiparametric empirical model of Laliberté,[92–94] recently extended in Ref. 133 for some other ions. From a microscopic viewpoint, not without an active and long-lived debate, it is enshrined in the literature that some species are able to enhance (structure maker ions or kosmotropes) or weaken (structure breaker ions or chaotropes, usually, big ions as Cs^+ or NO_3^-) the hydrogen bond strength.[134,135] However, predicting the influence on the viscosity of a certain ion requires one to understand the interplay among size, hydration, and polarizability of the chemical species in relation with these so-called Hofmeister effects, an issue that has been and still is under scrutiny in the field.[136,137] Moreover, experiments were in conflict in regard to the nature and intensity

of the perturbation of ions on the water "structure."[138–141] For instance, Corridoni *et al.*[101] established a robust structural parameter based on neutron diffraction experiments in a formal attempt to establish a relationship between the water structure and its effects on the viscosity of ionic solutions but claiming the effects of the ions in the H-bond network are independent on the ion, while, more recently, the differential effect of ions on the solvent H-bond has been proved by quasielastic neutron scattering experiments.[142]

After considering all this puzzling information, what can we learn from simulations? First, in Table IV we have incorporated the structural δ parameter defined in Ref. 101 to evaluate the predicted structure maker or breaker nature of the electrolyte as a whole, i.e., the kosmotropic/chaotropic balance. The values of δ are roughly constant with the concentration range, being precisely KNO_3, $RbNO_3$, $CsNO_3$, and NH_4NO_3 those monovalent salts within the selected set the ones with the smaller values of δ, in agreement with the kosmotropic behavior experimentally observed (see Fig. 4). Notice that, because NO_3^- acts as a structure breaker, the counterion might be strong enough to counterbalance their effect in the direction of increase in viscosity with concentration. In Fig. 4, the Molecular Dynamics results for the viscosities of the selected salts are presented, and it is apparent that this is only observed in the case of $NaNO_3$ [Fig. 4(a)], for which the curvature of the viscosity with concentration is accurately reproduced with the proposed force field with accuracy values below 8%. However, the smooth minimum at intermediate concentrations present for KNO_3 [Fig. 4(b)] becomes deeper in the alkali series. For KNO_3, we observed features akin to minimum, rough to be asserted within the computational uncertainties, but the viscosities are underestimated only by at most ~8%. As it will be discussed in Sec. III C 2, this minimum seems to be reliable provided the Stokes–Einstein relations is fulfilled. For $RbNO_3$ and $CsNO_3$ salts [depicted in Fig. 4(c)], a monotonous increment and a roughly constant viscosity value are predicted, with deviation from the experiments below 4%. This trend is expected because both Rb^+ and Cs^+ cations act as a significant structure breakers due to the high polarizability of ions and this points to assumption that nonpolarizable models are not able to capture the minimum in the viscosity–concentration plot for strong structure breaker salts, even when the simulated values of δ agree with the qualitative experimental behavior.

Because the minimum is rather smooth for NH_4NO_3, a nice quantitative agreement is also found for this salt [see Fig. 4(d), deviations below 4%], although, again, the minimum is not observed in simulations. This behavior aligns with the earlier discussed outcomes for polyatomic ions, where a better agreement was obtained using an ion charge of $\pm 0.85e$. Similar results are found for the divalent $(NH_4)_2SO_4$ salt. Since in the Madrid-2019 force field, the viscosities of sulfate salts were consistently underestimated and considering the reliable performance of the ammonium, we anticipate an underestimation of experimental viscosities for $(NH_4)_2SO_4$, as observed, with comparably higher deviations of ~10%.

Moreover, the structural parameter δ seems not to be useful in the prediction of viscosity variation with m either because of the stoichiometry of excluded volume reasons. When confronting an atomic ion of non-integer charge with a polyatomic ion, the effects of the distribution of charge in the latter can be palliated by tuning the ion–solvent interaction appropriately. However, if both ions are of polyatomic nature, the important Coulombic contribution to the potential energy should strongly depend on the value of the atomic charges. Thus, one may expect that if both charge distributions are not selected within the same method, the compensation obtained by the modification of the LJ part of the potential to the ion–ion and ion–solvent contributions might be insufficient to relieve the electrostatic interactions (particularly in multivalent species), and its potential influence on the predictions of dynamic and thermodynamic properties at a given concentration is hard to be anticipated. Moreover, as we pointed out in a recent study on the temperature of maximum in density,[45] the lack of polarization effects in the model also has influence on the reliability of the model to make quantitative predictions about salts comprised by highly polarizable species.

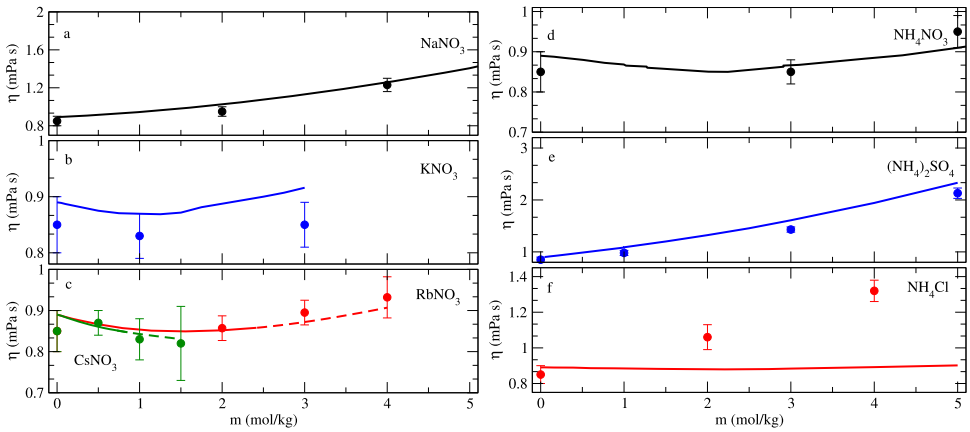

FIG. 4. Shear viscosity coefficients as a function of the molality for aqueous solutions of different nitrate and ammonium salts developed in this work. (a) $NaNO_3$, (b) KNO_3, (c) $RbNO_3$ and $CsNO_3$, (d) NH_4NO_3, (e) $(NH_4)_2SO_4$, and (f) NH_4Cl. Filled circles stand for simulation results, while continuous lines stand for the experimental data taken from Refs. 96 and 97 for $RbNO_3$ and $CsNO_3$ were extracted from, respectively, and from Refs. 92–94 for the rest of salts.

Nevertheless, for the NH_4Cl salt the experimental viscosity remains nearly constant across the entire concentration range, in agreement with a δ value close to zero. However, simulations do not predict such behavior and largely overestimate the experimental results. This discrepancy arises due to a complex interplay between the NH_4^+ cation, which attempts to reduce viscosity, and the Cl^- anion, which has a more dominant influence in increasing the viscosity coefficient when employing a charge of $\pm 0.85e$, as we have shown in previous works.[38,128,129] At this point, it is worth mentioning that assigning formal charges to electrolytes is artificial from a quantum perspective, since ion-to-solvent charge transfer events are known to dominate the water diffusivity in electrolytic solutions.[143–145] Since this chemical effect cannot be captured in classical force fields, including a dynamic charge is a desirable, yet computationally expensive, *effective* way of incorporating such effects into a classical simulation method. Nevertheless, the description of viscosity can be considered as quantitative in most cases, thus lengthening the applicability of the Madrid-2019 force field extended anew in this work for nitrogenated polyatomic ions.

2. Diffusion coefficients

Experimental values of the non-limiting diffusion coefficients of individual ions in water or water in the presence of ions are hard to be found in the literature. To the best of our knowledge, the only electrolytes comprised by NH_4^+ and/or NO_3^- for which there exist experimental data are NH_4Cl, KNO_3 and $(NH_4)_2SO_4$, reported by Tanaka[146] in the low concentration range ($m \leq 1$). These datasets will be our playground for testing the simulation data for diffusion coefficients. Before comparison, the calculated diffusion coefficients of water at various salt concentrations (D_{H_2O}) have to be corrected due to finite size effects as pointed out in previous works[147,148] and detailed in the Sec. II. Furthermore, experimental measurements of diffusion coefficients show a non-negligible degree of uncertainty. For instance, the diffusion coefficient of pure water reported in Ref. 149 is 2.3×10^{-5} cm^2/s, while the diffusion coefficient of pure water measured by Tanaka is close to 2.2×10^{-5} cm^2/s. To counterbalance these uncertainties, the experimental data were normalized by a factor 2.2×10^{-5} cm^2/s and the simulation outcomes by 2.3×10^{-5} cm^2/s, which corresponds to the corrected diffusion coefficient of water in the TIP4P/2005 model computed here.

Figure 5 illustrates the experimental normalized self-diffusion coefficients of water in solutions containing KNO_3, NH_4Cl, and $(NH_4)_2SO_4$ as continuous lines, while full symbols stand for the simulation results. The diffusion coefficients of KNO_3 exhibit remarkable agreement with the experimental results. The model successfully reproduces the experimentally observed increment of the diffusion coefficient, which represents a remarkable achievement, especially considering that, to the best of our knowledge, only *ab initio* Molecular Dynamics simulations of CsI solutions have previously reproduced an increasing trend of D with m.[150] Such degree of confidence is anticipated considering the application of the Stokes–Einstein relation and the favorable results achieved for viscosities using the newly optimized force field. In the case of NH_4Cl salts, the normalized diffusion coefficients of water in NH_4Cl solutions are significantly underestimated, a discrepancy that is consistent with the overestimation of the viscosity coefficient [as shown in Fig. 4(f)] and with the fault of self-diffusion of anions modeled within the Madrid-2019 force field

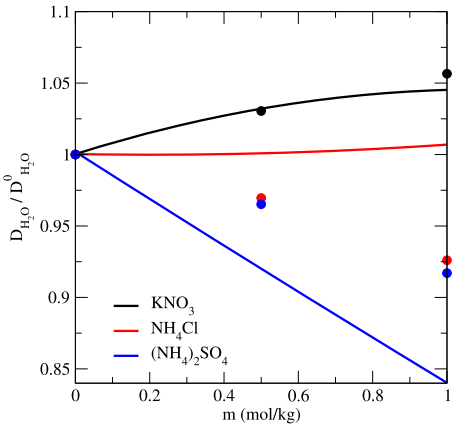

FIG. 5. Normalized self-diffusion coefficients of water in electrolyte solutions in the experimentally available concentration region. Simulation results are shown with filled circles. These data were corrected using the methodology proposed by Yeh and Hummer.[91] Solid lines are fits of the experimental data from Ref. 146.

(see Ref. 38). As previously highlighted, we have observed that the ammonium cation tends to yield accurate results for viscosity coefficients [see Figs. 4(d) and 4(e)]. Nonetheless, in the case of NH_4Cl, the viscosities were predominantly overestimated, primarily because of the presence of chloride anions. Our final case study involves the divalent $(NH_4)_2SO_4$ salt. The simulations show an overestimation of water diffusion coefficients in this solution, rougly consistent with the underestimate of the viscosities after considering the Stokes-Einstein relation. However, the disagreement is, on percentage terms, more important than those found in the predictions of viscosity coefficients. The reason of these deviations might be a dissimilar selection of the distribution of charge for polyatomic species. Another possible explanation could be that rotational degrees of freedom affect differently the diffusion coefficient values and the viscosities. It is clear that further work is needed to analyze the impact of ions having rotational degrees of freedom on transport properties such as viscosity or diffusion coefficients. Lastly, it is worth noting that despite the deviations observed in the last two salt cases with respect to experimental results, our findings effectively reproduce the order of experimental diffusion coefficients of water within the various studied electrolyte solutions, which follows the following sequence: $KNO_3 > NH_4Cl > (NH_4)_2SO_4$.

Finally, the self-diffusion coefficients of ions at infinite dilution are, however, well documented in the literature. For NO_3^- and NH_4^+, their values are $D^{\infty,exp}_{NO_3^-} = 1.90 \times 10^{-5}$ and $D^{\infty,exp}_{NH_4^+} = 1.98 \times 10^{-5}$ cm^2/s, respectively.[151] These values are not influenced by the presence of the counterion and are a good test of the performance of the force field in determining ion transport properties. The values of D^∞ were estimated by a linear extrapolation of the simulated values of D for NH_4NO_3 to $m \to 0$, and it was found that they are accurately reproduced: $D^{\infty,MD}_{NO_3^-} = 1.91 \times 10^{-5}$ cm^2/s (deviation of 0.5%) and $D^{\infty,MD}_{NH_4^+} = 1.91 \times 10^{-5}$ cm^2/s (deviation of 3.5%).

TABLE V. Summary of the simulation results for a ternary aqueous solution comprised by NH_4NO_3 (2 m) and NaCl (2 m) employing the Madrid-2019 (A) and the hybrid model described in the main text. For evaluating the Yeh–Hummer corrections to the diffusion coefficients, the shear viscosity was approximated as the average computed for each salt at 4 m concentration. The experimental value of the density was obtained by interpolating the experimental densities reported in Ref. 152. The experimental value of the diffusion coefficient of water was estimated from the experimental viscosities reported in Ref. 152 after appliying the Stokes-Einstein relation which implies that the product of viscosity and diffusion coefficient of water is the same in pure water and in the solution.

Model	ρ (kg/m^3)	$D_{H_2O} \cdot 10^5$ (cm^2/s)
A	1115.5	1.75
B	1115.9	1.91
Exp.	1116.7	1.93

D. Binary salt mixtures

Although we have focused on single salt solutions so far, in principle the force field proposed in this work should be able to deal with ternary system (i.e., water and two salts). Moreover, since experimental data on such ternary systems are scarce, simulations could help to provide some estimates of the thermodynamics properties of interest. Such an approach was followed in Ref. 37 for a few common mixtures. We performed additional simulations for a solution comprised by NH_4NO_3 2 m and NaCl 2 m (i.e., an electrolytic solution 4 m) at 298.15 K. In one simulation (A), the charge of all ions is set to $\pm 0.85e$ (Madrid-2019 force field). In the second simulation (B), we followed a hybrid model in which the charge of NH_4NO_3 was kept at $\pm 0.85e$ while those coming from the dissociation of NaCl are set to $\pm 0.75e$ (i.e., using the so-called Madrid-Transport model for NaCl). This selection of charge for NaCl is based on the previous experience of the group showing that for NaCl, the Madrid-Transport model provides an excellent description of densities, viscosities, and diffusion coefficients of water in the salt solution. The results for densities and diffusion coefficients are shown in Table V. The results for density were found to be very close, with the charge effect being noncritical (1115.45 kg/m^3 for A and 1115.87 kg/m^3 for B). The predictions for the density from simulations are in excellent agreement with the experimental result from Ref. 152 (see Table V). In the case of model B the prediction for the diffusion coefficient of water is also in excellent agreement with experiment. We hope that in the future the force field of this work can indeed provide reliable estimates of different properties for systems having two salts and water.

Although the density obtained with this hybrid force field (Madrid-2019 for NH_4NO_3 and Madrid-Transport for NaCl) is in agreement with that obtained for the Madrid-2019 force field for both salts, when using the charge $\pm 0.85e$ for NH_4NO_3 the viscosities of a 2 m solution are nicely predicted, but the value for a NaCl solution is slightly overestimated.[37] This suggests that the diffusion coefficient of water in the study of the ternary system could be underestimated. As observed in Table V and as anticipated in the text, a notable difference was observed in the diffusion coefficient of water in the solution when combining both models, with the value being ~13% higher when employing the Madrid-Transport model for NaCl. This fact indicates that combining both models is a feasible route for accurately describing the transport properties while maintaining precision in the evaluation of liquid densities. This opens the door to the study of ternary systems using different charges for different salts, provided they do not have a common ion.

In the case of solutions with salts with common ions, one can figure out that it has no physical meaning to have two "species" (in charge terms) for the same ion in a mixture, even when the system is electroneutral. We have found no simple recipe for how to proceed in this situation so far, although the possibility of describing the charge of a common ion in a sort of "mean field" approach could provide reasonable estimates. However, any possible guess coming from molecular simulations about the performance of this or other approximations should be speculative without any experimental data to be compared with.

IV. CONCLUSIONS

In this work, the Madrid-2019 force field has been extended to the polyatomic ions nitrate and ammonium. Although the models are built using the distribution of charge reported for OPLS models, the water–ion and ion–ion interactions were tuned either using the LB combining rules or by sidestepping them to improve the description of experimental results. Both the concentration dependence of the densities and the ion–ion and ion–solvent structures of the whole set of electrolyte solutions are in quantitative agreement when compared to experimental information, thus conferring enough precision upon the model for being of general applicability. The predictions of the solvent–ion structure are quite good, provided the strong intermolecular hydrogen bonding effects occurring in the complex coordination structure of the modeled ions. However, as expected for a scaled charge model with a net charge of $\pm 0.85e$, transport properties are not always nicely predicted, particularly when the counterion owns a marked kosmotropic character. It is foreseen that the experimental–simulation correspondence for viscosity coefficients might be potentially improved by tuning the global ion charge or charge distribution, as recently reported by some of us.[128] However, diffusion coefficients at infinite dilution are accurately reproduced, indicating that the global charge and charge distribution of the ions properly describe the ion–solvent potential energy surface. Despite this drawback, additional properties are expected to be correctly predicted with these models, such as the temperature of maximum in density,[44,45] the effect of the salt on the melting point of ice,[46] interfacial phenomena,[153] or the triple point temperature of hydrates in the presence of these electrolytes.[50] Such properties can be analyzed in future studies.

Overall, through combining the ability of the model to reproduce experimental behaviors for some salts and the drawbacks found for others, the tunable force fields proposed here constitute a valuable tool for unraveling the complex interactions that govern ion–water and ion–ion interactions in polyatomic electrolytes from a microscopic point of view and to strengthen the reliability and predictive capabilities of the model while providing a simple and accurate description for all densities, structure, and transport properties. Moreover, the confidence level provided by the proposed models paves the way for exploring either homogeneous or heterogeneous processes that are extremely important in the parametrization of aerosol contribution in general circulation models.[154]

SUPPLEMENTARY MATERIAL

In the supplementary material, we compile the numerical (raw data) and graphical information of the simulation results of all nitrate and ammonium salts considered in the main body of this work for the following properties: (i) the results for the Lennard-Jones parameters, σ_{ij} and ε_{ij} of the force field; (ii) simulation results for the density (ρ_{sim}) as a function of the molality (m); (iii) simulation results for the viscosity (η_{sim}) as a function of the molality (m); (iv) simulated atom–atom RDFs of interest for the whole set of electrolyte aqueous solutions considered in this work. We include a schematic representation of the expected RDF pattern for different types of ion–ion arrangements and of the geometrical features of the NO_3^- and NH_4^+ ions.

ACKNOWLEDGMENTS

V.M.T. acknowledges financial support provided by the Asociación Universitaria Iberoamericana de Postgrado (AUIP) under the program "Programa de Becas de Movilidad Académica AUIP 2024" and the Department of Physical Chemistry at the Universidad Complutense de Madrid for its hospitality. The authors are also thankful for funding received through the Ministerio de Ciencia e Innovación de España (Grant Nos. PID2022-136919NB-C31 and PID2022-136919NA-C33). We also thank the reviewers for useful comments.

AUTHOR DECLARATIONS

Conflict of Interest

The authors have no conflicts to disclose.

Author Contributions

V.M.T. and M.d.L contributed equally to this work.

Víctor M. Trejos: Data curation (equal); Formal analysis (equal); Investigation (equal). **Marcos de Lucas**: Data curation (equal); Formal analysis (equal); Investigation (equal). **Carlos Vega**: Conceptualization (supporting); Funding acquisition (equal); Methodology (equal); Writing – review & editing (equal). **Samuel Blazquez**: Formal analysis (equal); Investigation (equal); Methodology (equal); Writing – original draft (equal); Writing – review & editing (equal). **Francisco Gámez**: Conceptualization (equal); Funding acquisition (equal); Supervision (equal); Writing – original draft (equal); Writing – review & editing (equal).

DATA AVAILABILITY

The data that support the findings of this study are available within the article and its supplementary material.

REFERENCES

[1] *Nitrogen Cycle: Ecology, Biotechnological Applications and Environmental Impacts*, 1st ed., edited by J. Gonzalez-Lopez and A. Gonzalez-Martinez (CRC Press, 2021).
[2] E. Sanz-Luque, A. Chamizo-Ampudia, A. Llamas, A. Galvan, and E. Fernandez, "Understanding nitrate assimilation and its regulation in microalgae," Front. Plant Sci. **6**, 899 (2015).
[3] P. Lea, "Chapter 14 - ammonia assimilation and amino acid biosynthesis," in *Techniques in Bioproductivity and Photosynthesis*, 2nd ed., edited by S. L. J. Coombs, D. O. Hall, and J. Scurlock (Pergamon, 1985), pp. 173–187.
[4] B. H. S. G. Myhre, C. E. L. Myhre, and T. Storelvmo, "Aerosols and their relation to global climate and climate sensitivity," Nat. Educ. Know. **4**(5), 7 (2013).
[5] B. Elvers, S. Hawkins, and W. Russey, *Ullmann's Encyclopedia of Industrial Chemistry* (Wiley Online Library, 1989).
[6] V. Smil, "Detonator of the population explosion," Nature **400**(6743), 415 (1999).
[7] J. D. Bernal and R. H. Fowler, "A theory of water and ionic solution, with particular reference to hydrogen and hydroxyl ions," J. Chem. Phys. **1**, 515 (1933).
[8] W. L. Jorgensen, J. Chandrasekhar, J. D. Madura, R. W. Impey, and M. L. Klein, "Comparison of simple potential functions for simulating liquid water," J. Chem. Phys. **79**, 926–935 (1983).
[9] M. Mahoney and W. L. Jorgensen, "Quantum, intramolecular flexibility, and polarizability effects on the reproduction of the density anomaly of liquid water by simple potential functions," J. Chem. Phys. **115**, 10758–10768 (2001).
[10] H. J. C. Berendsen, J. R. Grigera, and T. P. Straatsma, "The missing term in effective pair potentials," J. Phys. Chem. **91**(24), 6269–6271 (1987).
[11] C. Vega and J. L. F. Abascal, "Simulating water with rigid non-polarizable models: A general perspective," Phys. Chem. Chem. Phys. **13**, 19663–19688 (2011).
[12] W. R. Smith, I. Nezbeda, J. Kolafa, and F. Moučka, "Recent progress in the molecular simulation of thermodynamic properties of aqueous electrolyte solutions," Fluid Phase Equilib. **466**, 19–30 (2018).
[13] J. Åqvist, "Ion-water interaction potentials derived from free energy perturbation simulations," J. Phys. Chem. **94**(21), 8021–8024 (1990).
[14] L. X. Dang, "Development of nonadditive intermolecular potentials using molecular dynamics: Solvation of Li^+ and F^- ions in polarizable water," J. Chem. Phys. **96**(9), 6970–6977 (1992).
[15] D. E. Smith and L. X. Dang, "Computer simulations of NaCl association in polarizable water," J. Chem. Phys. **100**(5), 3757–3766 (1994).
[16] Z. Peng, C. S. Ewig, M.-J. Hwang, M. Waldman, and A. T. Hagler, "Derivation of class II force fields. 4. van der Waals parameters of alkali metal cations and halide anions," J. Phys. Chem. A **101**(39), 7243–7252 (1997).
[17] S. Weerasinghe and P. E. Smith, "A Kirkwood–Buff derived force field for sodium chloride in water," J. Chem. Phys. **119**(21), 11342–11349 (2003).
[18] G. Lamoureux and B. Roux, "Absolute hydration free energy scale for alkali and halide ions established from simulations with a polarizable force field," J. Phys. Chem. B **110**(7), 3308–3322 (2006).
[19] J. Alejandre and J.-P. Hansen, "Ions in water: From ion clustering to crystal nucleation," Phys. Rev. E **76**(6), 061505 (2007).
[20] P. J. Lenart, A. Jusufi, and A. Z. Panagiotopoulos, "Effective potentials for 1:1 electrolyte solutions incorporating dielectric saturation and repulsive hydration," J. Chem. Phys. **126**(4), 044509 (2007).
[21] I. S. Joung and T. E. Cheatham, "Determination of alkali and halide monovalent ion parameters for use in explicitly solvated Biomolecular simulations," J. Phys. Chem. B **112**, 9020–9041 (2008).
[22] D. Corradini, M. Rovere, and P. Gallo, "A route to explain water anomalies from results on an aqueous solution of salt," J. Chem. Phys. **132**, 134508 (2010).
[23] K. M. Callahan, N. N. Casillas-Ituarte, M. Roeselová, H. C. Allen, and D. J. Tobias, "Solvation of magnesium dication: Molecular dynamics simulation and vibrational spectroscopic study of magnesium chloride in aqueous solutions," J. Phys. Chem. A **114**(15), 5141–5148 (2010).
[24] H. Yu, T. W. Whitfield, E. Harder, G. Lamoureux, I. Vorobyov, V. M. Anisimov, A. D. MacKerell, Jr., and B. Roux, "Simulating monovalent and divalent ions in aqueous solution using a Drude polarizable force field," J. Chem. Theory Comput. **6**(3), 774–786 (2010).
[25] M. M. Reif and P. H. Hünenberger, "Computation of methodology-independent single-ion solvation properties from molecular simulations. IV. Optimized Lennard-Jones interaction parameter sets for the alkali and halide ions in water," J. Chem. Phys. **134**(14), 144104 (2011).
[26] M. B. Gee, N. R. Cox, Y. Jiao, N. Bentenitis, S. Weerasinghe, and P. E. Smith, "A Kirkwood-Buff derived force field for aqueous alkali halides," J. Chem. Theory Comput. **7**(5), 1369–1380 (2011).

[27]S. Deublein, J. Vrabec, and H. Hasse, "A set of molecular models for alkali and halide ions in aqueous solution," J. Chem. Phys. **136**(8), 084501 (2012).
[28]S. Mamatkulov, M. Fyta, and R. R. Netz, "Force fields for divalent cations based on single-ion and ion-pair properties," J. Chem. Phys. **138**(2), 024505 (2013).
[29]F. Moučka, I. Nezbeda, and W. R. Smith, "Molecular force field development for aqueous electrolytes: 1. Incorporating appropriate experimental data and the inadequacy of simple electrolyte force fields based on Lennard-Jones and point charge interactions with Lorentz-Berthelot rules," J. Chem. Theory Comput. **9**, 5076–5085 (2013).
[30]P. T. Kiss and A. Baranyai, "A new polarizable force field for alkali and halide ions," J. Chem. Phys. **141**(11), 114501 (2014).
[31]R. Elfgen, M. Hülsmann, A. Krämer, T. Köddermann, K. N. Kirschner, and D. Reith, "Optimized atomistic force fields for aqueous solutions of magnesium and calcium chloride: Analysis, achievements and limitations," Eur. Phys. J. Spec. Top. **225**(8-9), 1391–1409 (2016).
[32]T. Yagasaki, M. Matsumoto, and H. Tanaka, "Lennard-Jones parameters determined to reproduce the solubility of NaCl and KCl in SPC/E, TIP3P, and TIP4P/2005 water," J. Chem. Theory Comput. **16**, 2460 (2020).
[33]A. Caruso, X. Zhu, J. L. Fulton, and F. Paesani, "Accurate modeling of bromide and iodide hydration with data-driven many-body potentials," J. Phys. Chem. B **126**(41), 8266–8278 (2022).
[34]D. Zhuang, M. Riera, G. K. Schenter, J. L. Fulton, and F. Paesani, "Many-body effects determine the local hydration structure of Cs^+ in solution," J. Phys. Chem. Lett. **10**(3), 406–412 (2019).
[35]J. Kim, Z. Wu, A. Morrow, A. Yethiraj, and A. Yethiraj, "Self-diffusion and viscosity in electrolyte solutions," J. Phys. Chem. B **116**, 12007–12013 (2012).
[36]Z. Kann and J. Skinner, "A scaled-ionic-charge simulation model that reproduces enhanced and suppressed water diffusion in aqueous salt solutions," J. Chem. Phys. **141**(10), 104507 (2014).
[37]I. M. Zeron, J. L. F. Abascal, and C. Vega, "A force field of Li^+, Na^+, K^+, Mg^{2+}, Ca^{2+}, Cl^-, and SO_4^{2-} in aqueous solution based on the TIP4P/2005 water model and scaled charges for the ions," J. Chem. Phys. **151**, 134504 (2019).
[38]S. Blazquez, M. M. Conde, J. L. F. Abascal, and C. Vega, "The Madrid-2019 force field for electrolytes in water using TIP4P/2005 and scaled charges: Extension to the ions F^-, Br^-, I^-, Rb^+, and Cs^+," J. Chem. Phys. **156**, 044505 (2022).
[39]I. V. Leontyev and A. A. Stuchebrukhov, "Electronic continuum model for molecular dynamics simulations," J. Chem. Phys. **130**, 085102(1)–085102(8) (2009).
[40]I. V. Leontyev and A. A. Stuchebrukhov, "Electronic continuum model for molecular dynamics simulations of biological molecules," J. Chem. Theory Comput. **6**, 1498–1508 (2010).
[41]I. V. Leontyev and A. A. Stuchebrukhov, "Polarizable mean-field model of water for biological simulations with AMBER and CHARMM force fields," J. Chem. Theory Comput. **8**, 3207–3216 (2012).
[42]B. J. Kirby and P. Jungwirth, "Charge scaling manifesto: A way of reconciling the inherently macroscopic and microscopic natures of molecular simulations," J. Phys. Chem. Lett. **10**(23), 7531–7536 (2019).
[43]E. Duboue-Dijon, M. Javanainen, P. Delcroix, P. Jungwirth, and H. Martinez-Seara, "A practical guide to biologically relevant molecular simulations with charge scaling for electronic polarization," J. Chem. Phys. **153**(5), 050901 (2020).
[44]L. F. Sedano, S. Blazquez, E. G. Noya, C. Vega, and J. Troncoso, "Maximum in density of electrolyte solutions: Learning about ion–water interactions and testing the Madrid-2019 force field," J. Chem. Phys. **156**(15), 154502 (2022).
[45]F. Gámez, L. F. Sedano, S. Blazquez, J. Troncoso, and C. Vega, "Building a Hofmeister-like series for the maximum in density temperature of aqueous electrolyte solutions," J. Mol. Liq. **377**, 121433– (2023).
[46]C. P. Lamas, C. Vega, and E. G. Noya, "Freezing point depression of salt aqueous solutions using the Madrid-2019 model," J. Chem. Phys. **156**, 134503 (2022).
[47]L. Perin and P. Gallo, "Phase diagram of aqueous solutions of LiCl: A study of concentration effects on the anomalies of water," J. Phys. Chem. B **127**, 4613 (2023).
[48]S. Blazquez, I. M. Zeron, M. M. Conde, J. L. F. Abascal, and C. Vega, "Scaled charges at work: Salting out and interfacial tension of methane with electrolyte solutions from computer simulations," Fluid Phase Equilib. **513**, 112548 (2020).
[49]G. Le Breton and L. Joly, "Molecular modeling of aqueous electrolytes at interfaces: Effects of long-range dispersion forces and of ionic charge rescaling," J. Chem. Phys. **152**(24), 241102 (2020).
[50]S. Blazquez, C. Vega, and M. Conde, "Three phase equilibria of the methane hydrate in NaCl solutions: A simulation study," J. Mol. Liq. **383**, 122031 (2023).
[51]S. Blazquez, J. Abascal, J. Lagerweij, P. Habibi, P. Dey, T. J. H. Vlugt, O. A. Moultos, and C. Vega, "Computation of electrical conductivities of aqueous electrolyte solutions: Two surfaces, one property," J. Chem. Theory Comput. **19**, 5380–5393 (2023).
[52]S. V. Sambasivarao and O. Acevedo, "Development of OPLS-AA force field parameters for 68 unique ionic liquids," J. Chem. Theory Comput. **5**, 1038–1050 (2009).
[53]B. Doherty, X. Zhong, S. Gathiaka, B. Li, and O. Acevedo, "Revisiting OPLS force field parameters for ionic liquid simulations," J. Chem. Theory Comput. **13**, 6131–6145 (2017).
[54]J. N. C. Lopes, J. Deschamps, and A. H. Pádua, "Modeling ionic liquids using a systematic all-atom force field," J. Phys. Chem. B **108**, 2038–2047 (2004).
[55]W. Jiang, T. Yan, Y. Wang, and G. A. Voth, "Molecular dynamics simulation of the energetic room-temperature ionic liquid, 1-hydroxyethyl-4-amino-1,2,4-triazolium nitrate (HEATN)," J. Phys. Chem. B **112**, 3121–3131 (2008).
[56]P. Salvador, J. E. Curtis, D. J. Tobias, and P. Jungwith, "Polarizability of the nitrate anion and its solvation at the air/water interface," Phys. Chem. Chem Phys. **5**, 3752–3757 (2003).
[57]D. Sorescu and D. Thompson, "Classical and quantum mechanical studies of crystalline ammonium nitrate," J. Phys. Chem. A **105**, 720–733 (2001).
[58]S. Jayaraman, A. P. Thompson, O. A. von Lilienfeld, and E. J. Maginn, "Molecular simulation of the thermal and transport properties of three alkali nitrate salts," Ind. Eng. Chem. Res. **49**, 559–571 (2010).
[59]M. Ribeiro, "On the Chemla effect in molten alkali nitrates," J. Chem. Phys. **117**, 266–276 (2002).
[60]M. C. González Lebrero, D. Bikiel, M. D. Elola, D. Estrin, and A. Roitberg, "Solvent-induced symmetry breaking of nitrate ion in aqueous clusters: A quantum-classical simulation study," J. Chem. Phys. **117**, 2718–2725 (2002).sssss
[61]A. Laaksonen and H. Kovacs, "Silver nitrate in aqueous solution and as molten salt: A molecular dynamics simulation and NMR relaxation study," Can. J. Chem. **72**, 2278–2285 (1994).
[62]H. Krienke and D. Opalka, "Hydration of molecular ions: A molecular dynamics study with a SPC/E water model," J. Phys. Chem. C **111**, 15935–15941 (2007).
[63]T. Megyes, S. Bálint, E. Peter, T. Grósz, I. Bakó, H. Krienke, and M. C. Bellissent-Funel, "Solution structure of $NaNO_3$ in water: Diffraction and molecular dynamics simulation study," J. Phys. Chem. B **113**, 4054–4064 (2009).
[64]G.-w. Lu, Y.-f. Li, W. Sun, and C.-x. Li, "Molecular dynamics simulation of hydration structure of KNO_3 electrolyte solution," Chin. J. Chem. Phys. **20**, 22–30 (2007).
[65]V. Fantauzzo, S. R. Yeandel, C. L. Freeman, and J. H. Harding, "A transferable force-field for alkali metal nitrates," J. Phys. Commun. **6**, 055011 (2022).
[66]V. Vchirawongkwin, H. Sato, and S. Sakaki, "RISM-SCF-SEDD study on the symmetry breaking of carbonate and nitrate anions in aqueous solution," J. Phys. Chem. B **114**(32), 10513–10519 (2010).
[67]V. Vchirawongkwin, C. Kritayakornupong, A. Tongraar, and B. M. Rode, "Symmetry breaking and hydration structure of carbonate and nitrate in aqueous solutions: A study by *ab initio* quantum mechanical charge field molecular dynamics," J. Phys. Chem. B **115**, 12527–12536 (2011).
[68]D. Schaefer, M. Kohns, and H. Hasse, "Molecular modeling and simulation of aqueous solutions of alkali nitrates," J. Chem. Phys. **158**, 134508 (2023).
[69]H. Krienke and G. Schmeer, "Hydration of molecular anions with oxygen sites – a Monte Carlo study," Z. Phys. Chem. **218**, 749–764 (2004).
[70]J. Heyda, M. Lund, M. Ončák, P. Slavíček, and P. Jungwirth, "Reversal of Hofmeister ordering for pairing of NH_4^+ vs alkylated ammonium cations with halide anions in water," J. Phys. Chem. B **114**, 10843–10852 (2010).
[71]A. Tongraar and S. Hannongbua, "Solvation structure and dynamics of ammonium (NH_4^+) in liquid ammonia studied by HF/MM and B3LYP/MM molecular dynamics simulations," J. Phys. Chem. B **112**, 885–891 (2008).
[72]K. P. Jensen and W. L. Jorgensen, "Halide, ammonium, and alkali metal ion parameters for modeling aqueous solutions," J. Chem. Theory Comput. **2**(6), 1499–1509 (2006).

[73]M. Liu, Q. Shi, and Z. Sun, "Molecular dynamics simulation of ammonium ion removal by freezing concentration," Nano Express **3**, 045005 (2023).
[74]A. Mondal and A. Sunda, "Molecular dynamics simulations of ammonium/phosphonium-based protic ionic liquids: Influence of alkyl to aryl group," Phys. Chem. Chem. Phys. **20**, 19268–19275 (2018).
[75]S. Mosallanejad, I. Oluwoye, M. Altarawneh, J. Gore, and B. Z. Dlugogorski, "Interfacial and bulk properties of concentrated solutions of ammonium nitrate," Phys. Chem. Chem. Phys. **22**, 27698–27712 (2020).
[76]J. Werner, E. Wernersson, V. Ekholm, N. Ottosson, G. Öhrwall, J. Heyda, I. Persson, J. Soderstrom, P. Jungwirth, and O. Bjorneholm, "Surface behavior of hydrated guanidinium and ammonium ions: A comparative study by photoelectron spectroscopy and molecular dynamics," J. Phys. Chem. B **118**, 7119–7127 (2014).
[77]D. van der Spoel, E. Lindahl, B. Hess, G. Groenhof, A. E. Mark, and H. J. C. Berendsen, "GROMACS: Fast, flexible, and free," J. Comput. Chem. **26**, 1701–1718 (2005).
[78]B. Hess, C. Kutzner, D. van der Spoel, and E. Lindahl, "GROMACS 4: Algorithms for highly efficient, load-balanced, and scalable molecular simulation," J. Chem. Theory Comput. **4**, 435–447 (2008).
[79]D. Beeman, "Some multistep methods for use in molecular dynamics calculations," J. Comput. Phys. **20**, 130–139 (1976).
[80]S. Nosé, "A molecular dynamics method for simulations in the canonical ensemble," Mol. Phys. **52**(2), 255–268 (1984).
[81]W. G. Hoover, "Canonical dynamics: Equilibrium phase-space distributions," Phys. Rev. A **31**, 1695–1697 (1985).
[82]M. Parrinello and A. Rahman, "Polymorphic transitions in single crystals: A new molecular dynamics method," J. Appl. Phys. **52**, 7182–7190 (1981).
[83]U. Essmann, L. Perera, M. L. Berkowitz, T. Darden, H. Lee, and L. G. Pedersen, "A smooth particle mesh Ewald method," J. Chem. Phys. **103**, 8577–8593 (1995).
[84]J. L. F. Abascal and C. Vega, "A general purpose model for the condensed phases of water: TIP4P/2005," J. Chem. Phys. **123**, 234505 (2005).
[85]B. Hess, H. Bekker, H. J. C. Berendsen, and J. G. E. M. Fraaije, "LINCS: A linear constraint solver for molecular simulations," J. Comput. Chem. **18**, 1463 (1997).
[86]B. Hess, "P-LINCS: A parallel linear constraint solver for molecular simulation," J. Chem. Theory Comput. **4**, 116–122 (2008).
[87]J. P. Ryckaert, G. Ciccotti, and H. J. C. Berendsen, "Numerical integration of the Cartesian equations of motion of a system with constraints. Molecular dynamics of *n*-alkanes," J. Comput. Phys. **23**, 327 (1977).
[88]W. L. Jorgensen and J. Gao, "Monte Carlo simulations of the hydration of ammonium and carboxylate ions," J. Phys. Chem. **90**, 2174–2182 (1986).
[89]W. M. Haynes, *CRC Handbook of Chemistry and Physics*, 95th ed. (CRC Press, 2014).
[90]M. A. González and J. L. F. Abascal, "The shear viscosity of rigid water models," J. Chem. Phys. **132**(9), 096101 (2010).
[91]I. C. Yeh and G. Hummer, "System-size dependence of diffusion coefficients and viscosities from molecular dynamics simulations with periodic boundary conditions," J. Phys. Chem. B **108**, 15873 (2004).
[92]M. Laliberte and W. E. Cooper, "Model for calculating the density of aqueous electrolyte solutions," J. Chem. Eng. Data **49**(5), 1141–1151 (2004).
[93]M. Laliberte, "Model for calculating the viscosity of aqueous solutions," J. Chem. Eng. Data **52**(2), 321–335 (2007).
[94]M. Laliberte, "A model for calculating the heat capacity of aqueous solutions, with updated density and viscosity data," J. Chem. Eng. Data **54**, 1725–1760 (2009).
[95]J. D'Ans, H. Surawski, and C. Synowietz, *Landolt-Bornstein. Numerical Data and Functional Relationships in Science and Technology* (Springer-Verlag Berlin Heidelllkrg, New York, 1977).
[96]H. G. Smith, J. H. Wolfenden, and H. Hartley, "LIV.—The viscosity and density of rubidium nitrate solutions," J. Chem. Soc. **1931**, 403–409.
[97]T. R. Merton, "CCLIII.—The viscosity and density of caesium nitrate solutions," J. Chem. Soc., Trans. **97**, 2454–2463 (1910).
[98]U. Patil and S. Keshri, "Unravelling the structural and dynamical properties of concentrated aqueous ammonium nitrate solutions: MD simulation studies," Mol. Simul. **49**, 1413–1430 (2023).
[99]M. T. H. Nguyen, O. Tichacek, H. Martinez-Seara, P. E. Mason, and P. Jungwirth, "Resolving the equal number density puzzle: Molecular picture from simulations of LiCl(aq) and NaCl(aq)," J. Phys. Chem. B **125**, 3153–3162 (2021).
[100]A. Lyubartsev and A. Laaksonen, "Concentration effects in aqueous NaCl solutions. A molecular dynamics simulation," J. Phys. Chem. **100**, 16410–16418 (1996).
[101]T. Corridoni, R. Mancinelli, M. A. Ricci, and F. Bruni, "Viscosity of aqueous solutions and local microscopic structure," J. Phys. Chem. B **115**, 14008–14013 (2011).
[102]P. A. Bergstroem, J. Lindgren, and O. Kristiansson, "An IR study of the hydration of perchlorate, nitrate, iodide, bromide, chloride and sulfate anions in aqueous solution," J. Phys. Chem. **95**(22), 8575–8580 (1991).
[103]G. Neilson and J. Enderby, "The structure around nitrate ions in concentrated aqueous solutions," J. Phys. C: Solid State Phys. **15**, 2347–2352 (1982).
[104]R. Caminiti, G. Licheri, G. Piccaluga, and G. Pinna, "On NO_3^-–H_2O interactions in aqueous solutions," J. Chem. Phys. **68**, 1967–1970 (1978).
[105]Y. Kameda, H. Saitoh, and O. Uemura, "The hydration structure of NO_3^- in concentrated aqueous sodium nitrate solutions," Bull. Chem. Soc. Jpn. **66**, 1919–1923 (1993).
[106]H. Liu, Y. Zhou, D. An, G. Wang, F. Zhu, and T. Yamaguchi, "Structure of aqueous KNO_3 solutions by wide-angle X-ray scattering and density functional theory," J. Phys. Chem. B **126**(31), 5866–5875 (2022).
[107]S. Dagnall, D. Hague, and A. Towl, "X-ray diffraction study of aqueous zinc(II) nitrate," J. Chem. Soc., Faraday Trans. 2 **78**, 2161–2167 (1982).
[108]E. R. Malinowski and P. S. Knapp, J. Chem. Phys. **48**, 4989–4991 (1968).
[109]A. Chialvo and L. Vlcek, "NO_3^- coordination in aqueous solutions by $^{15}N/^{14}N$ and $^{18}O/^{nat}O$ isotopic substitution: What can we learn from molecular simulation?," J. Phys. Chem. B **119**, 519–531 (2015).
[110]J. L. Thomas, M. Roeselová, L. X. Dang, and D. J. Tobias, "Molecular dynamics simulations of the solution–air interface of aqueous sodium nitrate," J. Phys. Chem. A **111**(16), 3091–3098 (2007).
[111]L. X. Dang, T.-M. Chang, M. Roeselova, B. C. Garrett, and D. J. Tobias, "On NO_3^-–H_2O interactions in aqueous solutions and at interfaces," J. Chem. Phys. **124**, 066101 (2006).
[112]W. J. Xie, Y. I. Yang, and Y. Q. Gao, "Dual reorientation relaxation routes of water molecules in oxyanion's hydration shell: A molecular geometry perspective," J. Chem. Phys. **143**(22), 224504 (2015).
[113]J. Thøgersen, J. Réhault, M. Odelius, T. Ogden, N. K. Jena, S. J. Knak Jensen, S. R. Keiding, and J. Helbing, "Hydration dynamics of aqueous nitrate," J. Phys. Chem. B **117**(12), 3376–3388 (2013).
[114]P. Banerjee, S. Yashonath, and B. Bagchi, "Rotation driven translational diffusion of polyatomic ions in water: A novel mechanism for breakdown of Stokes-Einstein relation," J. Chem. Phys. **146**(16), 164502 (2017).
[115]A. Tongraar, P. Tangkawanwanit, and B. M. Rode, "A combined QM/MM molecular dynamics simulations study of nitrate anion (NO_3^-) in aqueous solution," J. Phys. Chem. A **110**, 12918–12926 (2006).
[116]A. K. Pathak, T. Mukherjee, and D. K. Maity, "Microhydration of NO_3^-: A theoretical study on structure, stability and IR spectra," J. Phys. Chem. A **112**, 3399–3408 (2008).
[117]C. Ebner, R. Sansone, S. Hengrasmee, and M. Probst, "Molecular dynamics study of an aqueous potassium nitrate solution," Int. J. Quantum Chem. **75**, 805–814 (1999).
[118]H. Krienke, "On the influence of molecular structure on the conductivity of electrolyte solutions - sodium nitrate in water," Condens. Matter Phys. **16**, 43006 (2013).
[119]G. Szász and K. Heinzinger, "A Molecular Dynamics study of aqueous solutions. VIII. Improved simulation and structural properties of a NH_4Cl solution," Z. Naturforsch. A **34**, 840–849 (1979).
[120]F. Brugé, M. Bernasconi, and M. Parrinello, "Ab initio simulation of rotational dynamics of solvated ammonium ion in water," J. Am. Chem. Soc. **121**(47), 10883–10888 (1999).
[121]M. Ekimova, W. Quevedo, Ł. Szyc, M. Iannuzzi, P. Wernet, M. Odelius, and E. T. J. Nibbering, "Aqueous solvation of ammonia and ammonium: Probing

hydrogen bond motifs with FT-IR and soft X-ray spectroscopy," J. Am. Chem. Soc. **139**(36), 12773–12783 (2017).
[122]T.-M. Chang and L. X. Dang, "On rotational dynamics of an NH_4^+ ion in water," J. Chem. Phys. **118**(19), 8813–8820 (2003).
[123]G. Pálinkás, T. Radnai, G. Szász, and K. Heinzinger, "The structure of an aqueous ammonium chloride solution," J. Chem. Phys. **74**, 3522–3526 (1981).
[124]J. Guo, L. Zhou, A. Zen, A. Michaelides, X. Wu, E. Wang, L. Xu, and J. Chen, "Hydration of NH_4^+ in water: Bifurcated hydrogen bonding structures and fast rotational dynamics," Phys. Rev. Lett. **125**, 106001 (2020).
[125]H.-J. Böhm and I. McDonald, "An ab initio potential-energy function for $NH_4^+ \cdot H_2O$ and its use in the study of ionic coordination in solution," J. Chem. Soc., Faraday Trans. 2 **80**, 887–898 (1984).
[126]N. Hewish and G. Neilson, "Ammonium ion coordination in concentrated aqueous ammonium chloride," Chem. Phys. Lett. **84**(3), 425–427 (1981).
[127]A. H. Narten, "Diffraction pattern and structure of aqueous ammonium halide solutions," J. Phys. Chem. **74**(4), 765–768 (1970).
[128]S. Blazquez, M. Conde, and C. Vega, "Scaled charges for ions: An improvement but not the final word for modeling electrolytes in water," J. Chem. Phys. **158**(5), 054505 (2023).
[129]P. Habibi, A. Rahbari, S. Blazquez, C. Vega, P. Dey, T. Vlugt, and O. Moultos, "A new force field for OH^- for computing thermodynamic and transport properties of H_2 and O_2 in aqueous NaOH and KOH solutions," J. Phys. Chem. B **126**, 9376–9387 (2022).
[130]P. Habibi, J. R. Postma, J. T. Padding, P. Dey, T. J. Vlugt, and O. A. Moultos, "Thermodynamic and transport properties of $H_2/H_2O/NaB(OH)_4$ mixtures using the Delft force field (DFF/$B(OH)_4^-$)," Ind. Eng. Chem. Res. **62**, 11992 (2023).
[131]G. Jones and M. Dole, "The viscosity of aqueous solutions of strong electrolytes with special reference to barium chloride," J. Am. Chem. Soc. **51**, 2950–2964 (1929).
[132]H. Jenkins and Y. Marcus, "Viscosity B-coefficients of ions in solution," Chem. Rev. **95**, 2695–2724 (1995).
[133]J. Reynolds, B. Mauss, and R. Daniel, "The importance of ion interactions on electrolyte solution viscosities determined by comparing concentrated sodium carbonate and nitrate solutions," J. Mol. Liq. **288**, 111022 (2019).
[134]D. Yao, P. Tang, P. Song, and Z. Sun, "Viscosities and densities of mixed aqueous alkali metal nitrate solutions at T = (293.15–333.15) K," J. Chem. Eng. Data **67**, 2088–2097 (2022).
[135]D. E. Goldsack and R. Franchetto, "The viscosity of concentrated electrolyte solutions. I. Concentration dependence at fixed temperature," Can. J. Chem. **55**, 1062–1072 (1977).
[136]D. F. Parsons, M. Boström, T. J. Maceina, A. Salis, and B. W. Ninham, "Why direct or reversed Hofmeister series? Interplay of hydration, non-electrostatic potentials, and ion size," Langmuir **26**(5), 3323–3328 (2010).
[137]D. Parsons, M. Boström, P. L. Nostro, and B. W. Ninham, "Hofmeister effects: Interplay of hydration, nonelectrostatic potentials, and ion size," Phys. Chem. Chem. Phys. **13**, 12352–12367 (2011).
[138]R. Mancinelli, A. Botti, F. Bruni, M. Ricci, and A. Soper, "Perturbation of water structure due to monovalent ions in solution," Phys. Chem. Chem. Phys. **9**, 2959–2967 (2007).
[139]R. Mancinelli, A. Botti, F. Bruni, M. Ricci, and A. K. Soper, "Hydration of sodium, potassium, and chloride ions in solution and the concept of structure maker/breaker," J. Phys. Chem. B **111**, 13570–13577 (2007).
[140]I. Heisler, K. Mazur, and S. Meech, "Low-frequency modes of aqueous alkali halide solutions: An ultrafast optical Kerr effect study," J. Phys. Chem. B **115**, 1863–1873 (2011).
[141]A. Omta, M. Kropman, S. Woutersen, and H. Bakker, "Influence of ions on the hydrogen-bond structure in liquid water," J. Chem. Phys. **119**, 12457–12461 (2003).
[142]P. Luo, Y. Zhai, E. Senses, E. Mamontov, G. Xu, Y. Z, and A. Faraone, "Influence of kosmotrope and chaotrope salts on water structural relaxation," J. Phys. Chem. Lett. **11**, 8970–8975 (2020).
[143]M. Soniat and S. Rick, "The effects of charge transfer on the aqueous solvation of ions," J. Chem. Phys. **137**, 044511 (2012).
[144]Y. Yao, M. Berkowitz, and Y. Kanai, "Communication: Modeling of concentration dependent water diffusivity in ionic solutions: Role of intermolecular charge transfer," J. Chem. Phys. **143**, 241101 (2015).
[145]Y. Yao and Y. Kanai, "Free energy profile of NaCl in water: First-principles molecular dynamics with SCAN and ωB97X-V exchange-correlation functionals," J. Chem. Theory Comput. **14**, 884–893 (2018).
[146]K. Tanaka, "Measurements of self-diffusion coefficients of water in pure water and in aqueous electrolyte solutions," J. Chem. Soc., Faraday Trans. 1 **71**, 1127–1131 (1975).
[147]A. T. Celebi, S. H. Jamali, A. Bardow, T. J. H. Vlugt, and O. A. Moultos, "Finite-size effects of diffusion coefficients computed from molecular dynamics: A review of what we have learned so far," Mol. Simul. **47**, 831–845 (2021).
[148]S. H. Jamali, R. Hartkamp, C. Bardas, J. Sohl, T. J. H. Vlugt, and O. A. Moultos, "Shear viscosity computed from the finite-size effects of self-diffusivity in equilibrium molecular dynamics," J. Chem. Theory Comput. **14**(11), 5959–5968 (2018).
[149]K. Müller and H. Hertz, "A parameter as an indicator for water–water association in solutions of strong electrolytes," J. Phys. Chem. **100**(4), 1256–1265 (1996).
[150]Y. Ding, A. A. Hassanali, and M. Parrinello, "Anomalous water diffusion in salt solutions," Proc. Natl. Acad. Sci. U. S. A. **111**, 3310–3315 (2014).
[151]L. Yuan-Hui and S. Gregory, "Diffusion of ions in sea water and in deep-sea sediments," Geochim. Cosmochim. Acta **38**, 703–714 (1974).
[152]M.-F. Nowlan, T. Hoa Doan, and J. Sangster, "Prediction of the viscosity of mixed electrolyte solutions from single-salt data," Canadian J. Chem. Eng. **58**(5), 637–642 (1980).
[153]A. Benavides, M. Portillo, V. Chamorro, J. Espinosa, J. Abascal, and C. Vega, "Carlos, A potential model for sodium chloride solutions based on the TIP4P/2005 water model," J. Chem. Phys. **147**, 104501 (2017).
[154]K. Nordling, H. Korhonen, P. Räisänen, M. Alper, P. Uotila, D. O'Donnell, and J. Merikanto, "Role of climate model dynamics in estimated climate responses to anthropogenic aerosols," Atmos. Chem. Phys. **19**, 9969–9987 (2019).